machines

MDPI

Article

AutoML-Based Prediction of Process Outcomes in Expanded Polypropylene Autoclave Foaming

Enes Furkan Erkan

Department of Industrial Engineering, Sakarya University, Sakarya 54050, Türkiye; eneserkan@sakarya.edu.tr

Abstract

The foam injection molding process for expanded polypropylene (EPP) offers advantages in energy efficiency, material savings, and mechanical performance, making it suitable for automotive and packaging applications. However, its nonlinear and multivariable nature makes accurate prediction and process optimization difficult using traditional methods. This study presents an AutoML-based surrogate modelling framework for predicting and optimizing two key process outcomes: cycle time and warpage. Experimental data were obtained from 81 production trials conducted on a Teubert injection molding machine using five process parameters. The PyCaret library was used to automate model selection, hyperparameter tuning, and performance evaluation, and 18 regression algorithms were compared. The results showed that tree-based ensemble models clearly outperformed traditional linear models. Gradient Boosting Regressor achieved an R^2 of 0.9671 for cycle time, while Extra Trees Regressor reached an R^2 of 0.9874 for warpage. Beyond prediction, the finalized surrogate models were used for Monte Carlo-based design space exploration with 1000 synthetic parameter combinations. Non-dominated solutions were identified to construct the Pareto front, and the top-ranked settings were compared with experimental results. The findings show that AutoML-based surrogate modelling can support both accurate prediction and process window identification in EPP foam injection molding.

Keywords: AutoML; expanded polypropylene; foam injection; machine learning

1. Introduction

The foam injection process involves introducing a physical blowing agent (such as CO_2 or N_2) into molten thermoplastic resin to create a microcellular structure. This technique is widely used in the production of automotive interior trim parts, packaging, white goods, and electronic components. It offers notable advantages, including 10–35% savings in raw material usage, a 25–50% reduction in pressing pressure, and a significant decrease in environmental impact [1–4]. Effective control of the cell structure enhances thermal and acoustic insulation while preserving critical levels of impact and tensile strength. It also reduces energy consumption by up to 40% through shortened processing times [2,4]. Life cycle assessment studies indicate approximately a 15% reduction in environmental impact for plant fiber-reinforced polypropylene composites, while CO_2-based physical foaming significantly lowers the carbon footprint [1,4,5]. However, if key process parameters such as gas pressure, mold temperature, and cooling time are not properly managed in critical or low-pressure gas injection, defects such as poor surface quality, cell heterogeneity, and inconsistent mechanical properties may arise. Consequently, data-driven

Academic Editor: Shohin Aheleroff

Received: 7 June 2026
Revised: 10 July 2026
Accepted: 13 July 2026
Published: 14 July 2026

modelling and prediction approaches supported by design of experiments (DOE), numerical simulations, and machine learning are essential for improving process behaviour [6,7].

Positioning AutoML relative to classical Design of Experiments (DOE), combined with machine learning (ML) hybrid approaches, highlights distinct advantages and limitations for each methodology. AutoML automates model selection, hyperparameter optimisation, and, in many cases, feature engineering, thereby offering substantial gains in efficiency and ease of use, particularly in applications that require rapid deployment with minimal human intervention [8]. This advantage is especially pronounced in complex multi-target prediction tasks, where AutoML frameworks can standardise and streamline the modelling workflow across diverse problem settings [8]. By contrast, DOE–ML hybrid approaches rely on the systematic experimental design principles of DOE to generate structured, informative datasets that are subsequently used to train ML models. This strategy is particularly effective when domain knowledge can be explicitly incorporated into the experimental design and modelling process, thereby improving both predictive performance and interpretability [9].

Expanded polypropylene (EPP) is a key material in various industries, including automotive, packaging, and consumer products. Due to its properties, such as high impact strength, energy absorption, and dimensional stability in foam injection processes. Its cellular structure enables the production of lightweight components without compromising mechanical performance, despite its low density. EPP is particularly favoured in the automotive sector for applications such as side impact protectors, bumper fillers, and interior trim components. It is also widely used in reusable packaging thanks to its multi-impact resistance [10,11]. Moreover, its high thermal insulation capacity and chemical resistance make it suitable for energy-efficient manufacturing techniques, including steam-chest molding [3]. EPP samples with a density of 60 kg/m^3 demonstrate 245% higher compressive strength and absorb 187% more energy than those with a density of 20 kg/m^3 [12]. EPP emerges as a strategic material for enhancing sustainability, impact safety, and production efficiency in foam injection technologies. Expanded polypropylene in its granular form is presented in Figure 1.

In the literature, research on the foam injection process of EPP primarily focuses on evaluating the material's dynamic impact and compression behaviour using split-Hopkinson pressure bar (SHPB) tests [13,14]. Studies addressing process parameter effects are predominantly based on traditional experimental and data-driven modelling approaches, such as experimental design of experiments [15,16], the Taguchi method [17], and regression analyses [18]. Although numerous optimization studies have been conducted on plastic injection processes, research specifically targeting the EPP process remains limited. While a few studies have addressed the properties of EPP beads, material strength, and recyclability, there is a notable lack of research focusing on systematic and automated predictive modelling frameworks. In study [17], key process parameters for EPP were identified using the Taguchi method, followed by predictive modelling using various artificial neural network approaches. However, the inherent complexity of the production process and the numerous influencing variables highlight the need for more comprehensive and systematic research in this area.

Figure 1. EPP material.

In recent years, artificial intelligence-based approaches have offered significant advantages in the modelling and performance assessment of production processes. While classical machine learning methods have been widely applied to analyse complex, multivariable systems in the manufacturing sector, their effectiveness often relies heavily on expert intervention and trial and error [19]. Uncertainties, particularly in hyperparameter tuning and algorithm selection, render the model development process both time-consuming and costly [20]. As a result, AutoML methods have gained prominence in production domains where reliable and reproducible predictive models are critical, such as foam injection processes. AutoML approaches enhance the accuracy and robustness of models by autonomously managing hyperparameter tuning and model selection, thereby supporting process improvement through more accurate prediction and reduced experimental effort [21,22]. In this context, this study aims to address the limitations of traditional methods by employing AutoML techniques to develop accurate surrogate models for predicting key process outcomes in foam injection, thereby providing a systematic and comprehensive evaluation within this application domain. The flowchart of the study is presented in Figure 2.

The remainder of this paper is organised as follows: Section 2 presents a comprehensive review of the related literature. Section 3 describes the materials and methods used in the experimental setup and provides detailed information on the AutoML framework adopted in the study. Section 4 discusses the results and key findings, while Section 5 concludes the paper with final remarks and future research directions.

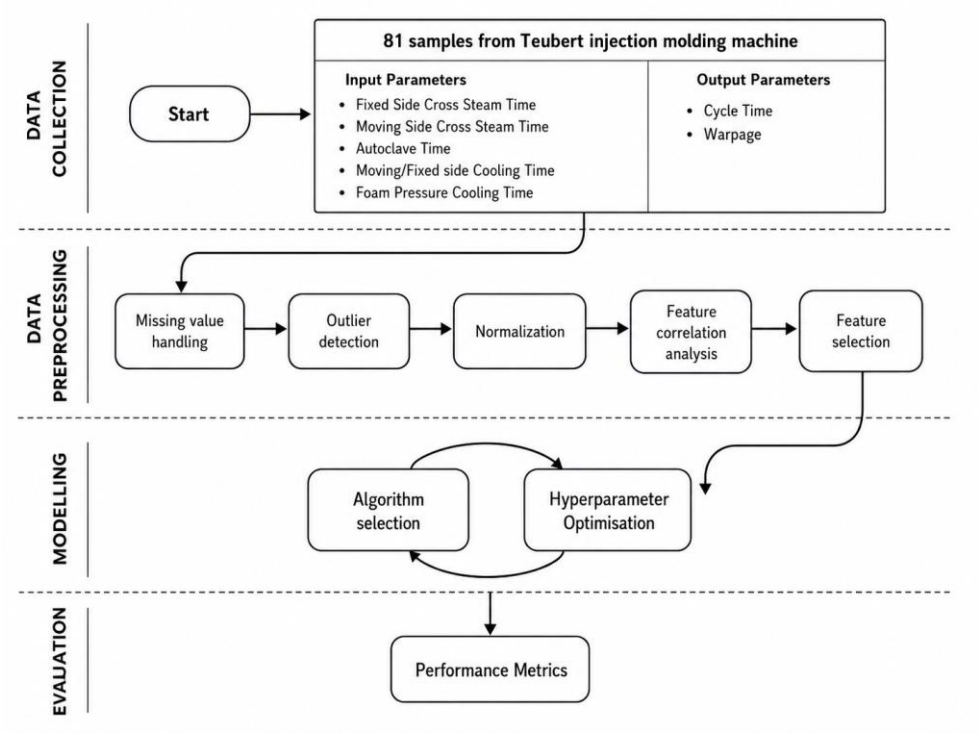

Figure 2. Flow diagram of the study.

2. Literature Review

EPP is a lightweight and versatile thermoplastic foam commonly used in packaging, automotive, and consumer goods due to its energy absorption and low density. The application of machine learning techniques to the injection molding process of EPP foams presents significant opportunities to enhance production efficiency, improve quality prediction, and minimise material waste.

Recent studies illustrate the broad adoption of advanced machine-learning paradigms across different application domains. For example, Ashraf et al. proposed an attention-based framework to improve micro-expression recognition, demonstrating the effectiveness of attention mechanisms for enhancing feature discrimination and robustness [23]. Similarly, Khubaib et al. introduced a data-efficient shifted window transformer for wheat disease detection, highlighting the importance of architectures that maintain strong performance under limited data [24]. From the perspective of transparency and trust, Kehkashan et al. developed an explainable phishing website detection approach, emphasizing the growing role of explainability in practical machine-learning systems [25]. In the medical imaging domain, Azeem et al. demonstrated the effectiveness of SSD- and YOLO-based detectors for detecting diabetic foot ulcers, further confirming the impact of deep learning and ensemble learning strategies in safety-critical applications [26]. Although these studies address different problems, they collectively underline key trends such as automation, data efficiency, robustness, and explainability. In this context, the present work extends these methodological advances to the injection molding domain through an AutoML-driven, ensemble-based modelling framework.

The application of machine learning in the injection molding industry has become increasingly critical, particularly in quality control, process monitoring and prediction, and process optimization. Numerous studies have shown that machine learning algorithms can effectively predict common defects such as warpage, short shots, and sink marks, which frequently occur during the injection molding process [27–29]. Ke et al. developed an advanced machine learning model incorporating an autoencoder for quality prediction, demonstrating high predictive accuracy, reduced scrap rates, and enhanced

production sustainability [30]. These findings are consistent with prior research highlighting the importance of real-time monitoring and predictive analytics in maintaining process integrity and operational efficiency [31].

Recent advancements in rapid molding technologies have significantly reduced production times in the injection molding industry. Studies have shown that injection molds fabricated with aluminium-filled epoxy resins can notably shorten cycle times compared to conventional steel-based molds, thereby enhancing overall production efficiency [32,33]. These technological improvements contribute to sustainable development goals by increasing operational efficiency while reducing energy consumption and material waste [34]. Moreover, the integration of rapid manufacturing processes with artificial intelligence is fostering the development of innovative methodologies to achieve fast, cost-effective, and high-quality production outputs [35,36], where data-driven prediction models play a central role in supporting informed decision-making.

The integration of simulation tools with artificial intelligence significantly enhances the analysis and prediction of process behaviour in injection molding. By combining machine learning algorithms with molding simulations, manufacturers can accelerate the validation of mold designs through the implementation of digital twin technologies [36]. This integrated approach enables better management of temperature and pressure fluctuations during production, which are critical factors influencing the mechanical properties of the final product [37]. Data-driven models further support precise tuning of process conditions to ensure consistent performance within defined tolerances [38].

Pacella et al. investigate the use of regression models to cluster energy consumption patterns in injection molding, demonstrating that predictive analytics can substantially improve energy efficiency. Transitioning from traditional energy-intensive methods to data-centric approaches enables more informed decisions regarding resource allocation and consumption [39,40]. These improvements contribute to both economic and environmental sustainability, which are essential priorities in modern manufacturing.

Selvaraj et al. argue that although the initial implementation costs of artificial intelligence and machine learning systems in injection molding may be substantial, the long-term productivity benefits are particularly evident in high-volume production settings. The efficiency gains offered by these technologies justify the initial investment, as they can result in significant reductions in labour and material costs over time [28]. Within this context, the application of machine learning enhances production agility and precision, attributes that are especially critical in industries requiring rapid turnaround without compromising quality, with predictive modelling serving as a key enabler of such improvements.

Despite these advancements, a review of the literature reveals a notable gap in the application of machine learning algorithms specifically to EPP foam injection molding processes. Integrating machine learning into EPP foam injection molding processes has the potential to improve manufacturing efficiency, enhance quality assurance, and support sustainable practices, particularly through the development of robust AutoML-based prediction models. The studies reviewed emphasize the transformative role of AI in advancing operational excellence. As the field progresses, it is essential for researchers and industry professionals to remain engaged with these developments and pursue innovative, data-driven solutions to meet evolving production demands and sustainability goals.

3. Materials and Methods

3.1. Overview of the EPP Foam Injection Sequence

The molding process begins by pneumatically feeding pre-expanded EPP beads, which possess a constant density of 21 g/L, into the closed mold cavity. The molding phase then proceeds sequentially: First, cross-steaming is applied from the fixed side to the mov-

https://doi.org/10.3390/machines14070797

ing side (P1), and then in reverse (P2), to ensure the internal fusion and bonding of the beads. This is followed by an autoclave step (P3), where steam is injected simultaneously from both sides without exhaust to improve structural homogeneity and surface quality. Next, water is sprayed into the cooling channels of both mold halves (P4) to solidify the product and provide the dimensional stability required for demolding. Finally, a pressure stabilization period (P5) allows the internal foam pressure to drop to a safe level, relieving internal stresses before the mold opens and the final part is ejected. A schematic representation of a typical EPP mold is given in Figure 3.

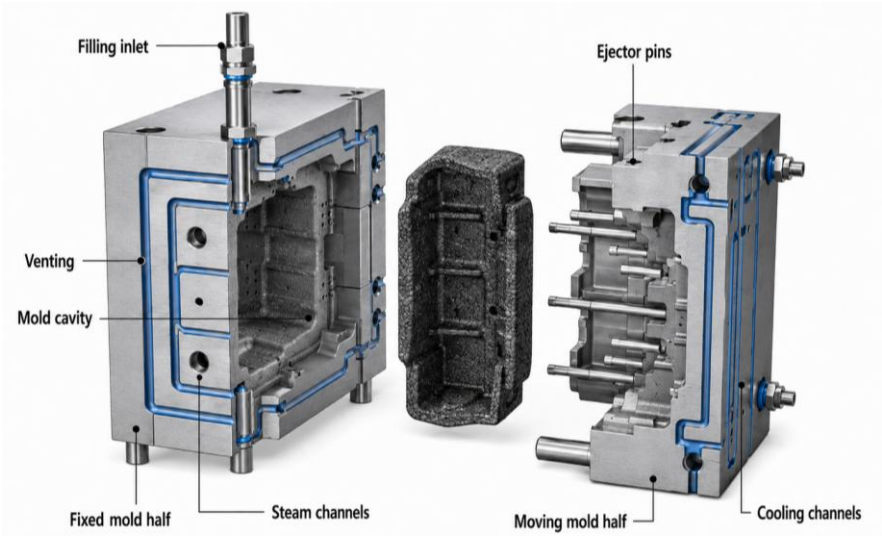

Figure 3. Schematic representation of a typical EPP mold structure.

3.2. Data Collection

The experimental data used in this study were obtained from applications conducted using a Teubert injection molding machine. The data were sourced from studies presented in [17]. A total of 81 samples were collected under controlled process conditions and recorded for analysis. Five key process parameters influencing the machine's production performance were examined, with cycle time and warpage measurements used as system outputs. The recorded cycle time represents the complete automated machine cycle rather than a simple mathematical sum of the static parameter inputs. It specifically incorporates the dynamic in-mold cooling and pressure equalization phases. Because the required duration for pressure stabilization depends strictly on the initial thermal inputs and the cooling efficiency required to relieve internal stresses, it is not a fixed machine setup value. Therefore, the total cycle time is inherently linked to the foaming quality and is evaluated as a dynamic output variable in this study. Descriptions and identification numbers of these parameters are provided in Table 1. The selection of these five specific parameters (P1–P5) was based on a comprehensive preliminary screening. Initially, 11 potential process parameters adjusted by operators during production (including automatic clamp pressures for moving/fixed sides, filling pressures, etc.) were evaluated. Based on a Taguchi orthogonal array and Analysis of Variance (ANOVA), parameters such as clamp and filling pressures were found to have no statistically significant effect on warpage or cycle time ($p > 0.05$). Consequently, they were kept constant within standard machine limits, and the modelling framework was built exclusively on P1–P5, which had the strongest influence on the process outcomes. The primary objective of this study is to develop and evaluate data-driven predictive models that can accurately estimate critical quality and performance indicators. In this context, the dataset is used to construct an AutoML-based modelling framework that supports informed decision-making and reduces the need for

extensive trial-and-error experiments in production planning. EPP was used as the raw material in the production process, with a density of 21 g/L.

Table 1. Model parameters and descriptions.

No	Parameter	Explanation
P1	Fixed Side Cross Steam Time (s)	The mold's stationary portion, known as the "fixed side," is usually stronger and more stable. Steam is injected from the fixed side of the mold and moves toward the movable side during cross steaming. The movable side exhausts the condensate. Internal fusing within the portion is encouraged by this process.
P2	Moving Side Cross Steam Time (s)	The side of the mold that opens and closes while the injection process is underway is referred to as the movable side. Steam is directed from the movable side of the mold toward the fixed side when cross steaming is taking place on the movable side. The fixed side exhausts the condensate. Internal fusing within the portion is facilitated by this process.
P3	Autoclave Time (s)	During the autoclave stage, steam is applied simultaneously from both the fixed and movable sides of the mold, with no steam exhaust occurring during the process. This step enhances the surface quality of the part, ensures uniformity, and improves its overall strength.
P4	Moving/Fixed Side Cooling Time (s)	This parameter defines the cooling duration applied to both the fixed and moving sides of the mold, ensuring the product reaches the appropriate temperature for smooth and defect-free demolding. Inadequate cooling time increases the risk of deformation, while excessive cooling results in unnecessary downtime and reduced production efficiency.
P5	Foam Pressure Cooling Time (s)	This step allows the part to stabilize by relieving internal stress. No water or steam is injected into the mold, and the condensate outputs stay open. At this point, the internal foam pressure can drop to the desired level.
-	Cycle Time (Output Variable)	It is the time required to complete a production process from beginning to end.
-	Warpage (Output Variable)	After the molding process, the plastic part undergoes uneven or undesirable deformation due to internal stresses in different areas during the cooling process.

Figure 4 presents representative images from the warpage measurement performed as part of the quality assessment of the EPP component. To ensure measurement standardization and repeatability, the manufactured parts underwent an 8 h oven-curing process, an industrially applied stabilization procedure for the EPP cellular expansion and shrinkage dynamics to fully stabilize. Warpage was subsequently measured using a triangular ruler on an 11-point checking fixture specifically designed for the part geometry. The measurement from the most critical deformation point relative to the reference surface was selected as the target variable for model training.

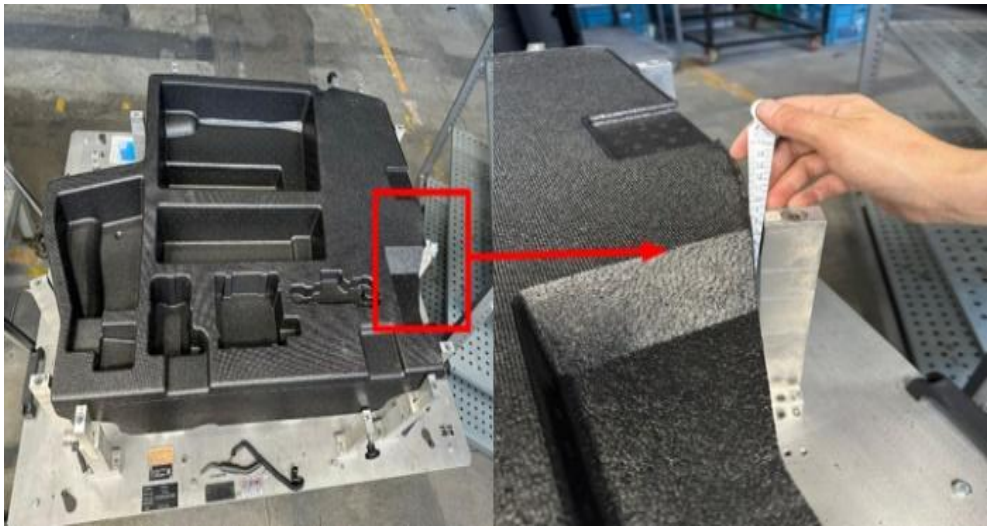

Figure 4. Warpage measurement images for quality assessment of the EPP component.

3.3. Data Preparation

The 81-sample dataset was systematically generated using a Taguchi L27 fractional factorial design, which evaluates the 5 selected parameters at 3 levels each [17]. This design was repeated three times to ensure statistical reliability. Therefore, the clustered distribution observed in the histograms is a direct mathematical consequence of this discrete experimental design rather than arbitrary sampling. Statistical analysis of the dataset confirms that the input parameters (P1–P5) and the output variables (Cycle Time and Warpage) are well distributed within the ranges defined in Table 2. Notably, parameters P4 and P5 exhibit the highest variability (std = 8.21), suggesting they may exert a more significant influence on process performance compared to other inputs. The observed ranges in the system outputs—167.8 to 208.3 s for Cycle Time and 10.1 to 15.9 mm for Warpage—indicate that the experimental design provides a sufficient range of process conditions to capture the impact of parameter variations on the final product quality.

Table 2. Basic statistical information of the database.

	P1	P2	P3	P4	P5	Cycle Time	Warpage
Levels	4, 5.5, 7	4, 5.5, 7	9, 10, 11	65, 75, 85	30, 40, 50	-	-
mean	5.50	5.50	10	75	40	187.31	14.08
std	1.23	1.23	0.82	8.21	8.21	11.06	1.66
min	4	4	9	65	30	167.8	10.10
max	7	7	11	85	50	208.3	15.90

To assess experimental reliability, noise levels were calculated using repeated observations for identical parameter combinations. The results show low average noise levels for both Cycle Time (0.0795) and Warpage (0.0607), with limited dispersion, confirming high repeatability and consistency of the experimental setup. The presence of zero noise values in some cases indicates consistent repeated measurements rather than data quality issues. These low noise levels indicate a high signal-to-noise ratio, which is generally advantageous for machine learning applications, as it facilitates the learning of underlying process relationships rather than stochastic variations [41].

Figure 5 illustrates the distribution of the five input parameters (P1–P5) used in the experimental study. Because the dataset was systematically generated using a Taguchi L27 fractional factorial design, each parameter was tested at exactly three predetermined levels. Consequently, the histograms show that the data points are strictly clustered at

these specific intervals. This plot is provided to visually confirm the discrete, factorial-based structure of the experimental design and to contrast it with continuous random sampling. This approach enables a more controlled and consistent analysis of parameter effects. Moreover, it eliminates the need for resampling or data balancing during pre-processing, allowing the analysis to proceed directly within the experimental design.

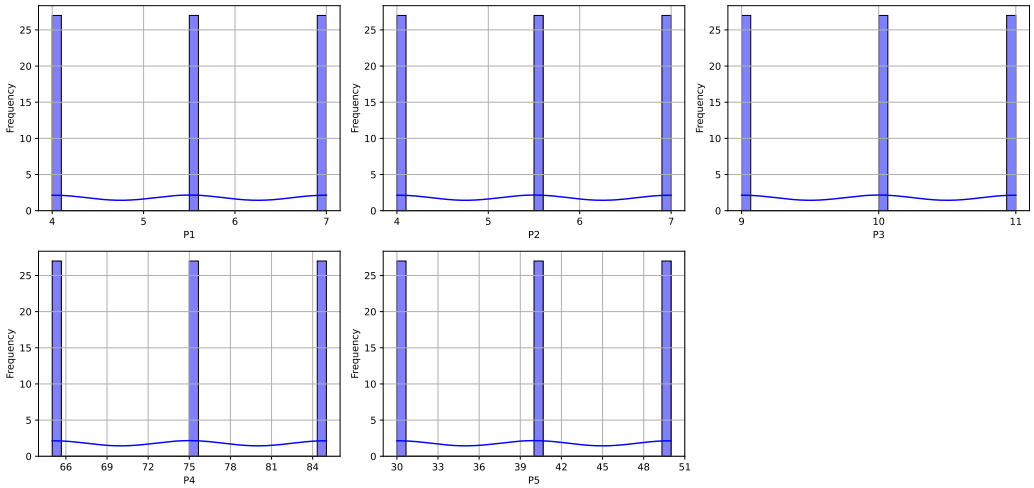

Figure 5. Distribution of inputs.

Figure 6 displays the distributions of Cycle Time and Warpage, two key performance indicators of the production process. Analysis of the histograms and density curves reveals that Cycle Time exhibits a broad and irregular distribution ranging from 170 to 210 s, indicating a deviation from normality. This suggests that the influence of process parameters on Cycle Time is heterogeneous, resulting in varying responses across different parameter combinations. In contrast, the distribution of Warpage is more asymmetrical, with data clustered around 15 mm and higher frequencies observed in this range. This pattern indicates that the system is more susceptible to warpage under certain conditions, with potential quality risks concentrated in this region.

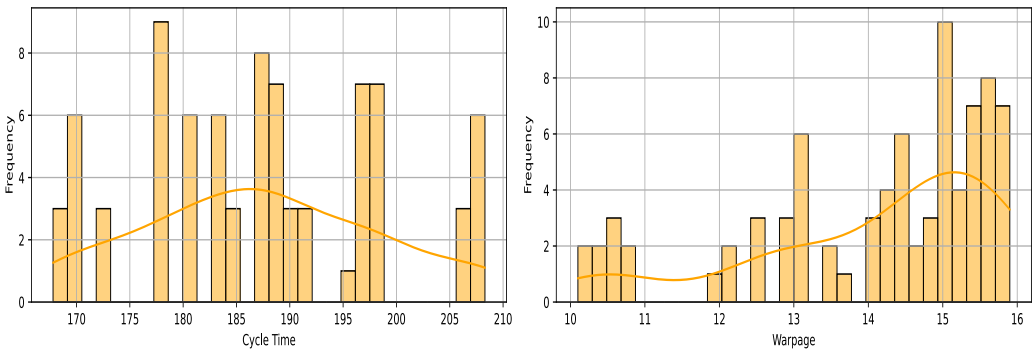

Figure 6. Distribution of outputs.

Figure 7 presents the results of a multivariate outlier analysis based on the variables Cycle Time and Warpage. Using the Mahalanobis distance, the analysis showed that the majority of the samples conformed to the dataset's overall structure, with no statistical outliers detected. The absence of red-marked points in the graph indicates that none of the samples were identified as outliers according to the Mahalanobis distance criteria. This

confirms the dataset's homogeneity and supports its suitability for subsequent modelling and analytical procedures.

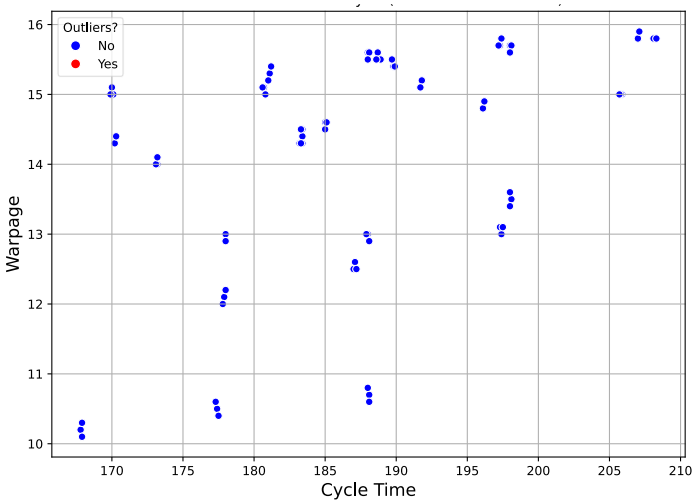

Figure 7. Multivariate outlier analysis.

The correlation matrix presented in Figure 8 illustrates the relationships among the variables used in the modelling process. Parameters P4 and P5 exhibit positive correlations with both Cycle Time (r = 0.66 and r = 0.70, respectively) and Warpage (r = 0.51 and r = 0.13, respectively), suggesting that these two inputs play a significant role in influencing process performance. Moreover, the lack of strong correlations among the input variables indicates minimal multicollinearity, which is favourable for model stability and interpretability, particularly in regression-based approaches. Overall, the analysis confirms that the dataset possesses both high explanatory capacity and input independence, making it suited for application in machine learning algorithms.

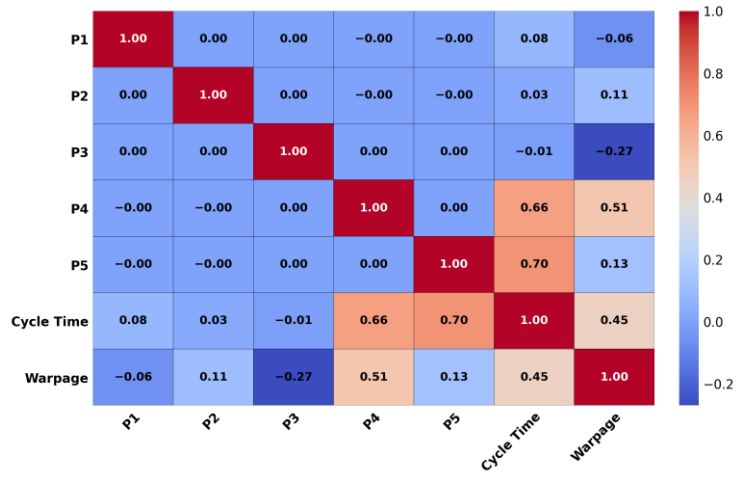

Figure 8. Correlation matrix.

3.4. AutoML

In this study, model tuning was performed using 5-fold cross-validation to ensure reliable performance evaluation [42]. The hyperparameters of each model were adjusted within this validation framework, and performance was assessed using various metrics. To ensure consistency and reproducibility, a fixed random seed was used throughout the process. This methodology enabled a fair comparison and ranking of the algorithms based

on their performance metric results, providing reliable insights into their effectiveness [43].

With advances in computational power, machine learning aims to enable systems to learn from data and make inferences in a manner like human reasoning. The primary goal is to train models on experimental datasets, generate predictions, and systematically evaluate their generalization performance. Machine learning algorithms are designed to identify patterns and relationships within input data to support decision-making processes [44,45].

Recent innovations in low-code platforms and AutoML have significantly simplified and accelerated the development of machine learning models [46,47]. Low-code platforms allow users with minimal programming experience to participate in application development, while AutoML automates key stages of the machine learning pipeline, including data preprocessing, model selection, and hyperparameter tuning. These technologies primarily facilitate rapid model development and objective model comparison, making machine learning more accessible to a broader range of users.

This study employs the Python version 3.10.20-based PyCaret version 3.3.2 library, a user-friendly AutoML that streamlines the machine learning workflow. PyCaret facilitates comparison of multiple algorithms, provides detailed performance metrics, and helps identify the most accurate regression model for a given dataset [48]. The library supports a wide array of regression algorithms, including Gradient Boosting Regressor, Random Forest Regressor, Extra Trees Regressor, Huber Regressor, Linear Regression, Least Angle Regression, Lasso Regression, Lasso Least Angle Regression, Decision Tree Regressor, CatBoost Regressor, Ridge Regression, Passive Aggressive Regressor, Bayesian Ridge, Orthogonal Matching Pursuit, Elastic Net, K Neighbors Regressor, Light Gradient Boosting Machine, Dummy Regressor, and AdaBoost Regressor. This diverse set of models enables a comprehensive evaluation of algorithmic performance within the context of foam injection process optimization.

3.5. Performance Metrics

In this study, the following performance metrics are employed to evaluate the predictions of cycle time and warpage. These metrics are important for assessing the efficiency and reliability of the developed models. Deviations between the actual and predicted values are calculated and interpreted for each selected performance indicator.

- Mean Absolute Error (MAE)

The MAE is calculated by averaging the absolute differences between the predicted and actual values. As a straightforward and unambiguous measure of error magnitude, MAE directly reflects the size of the prediction errors without requiring further interpretation. Due to its sensitivity to scale, it is widely used in evaluations involving dimensional data and is commonly preferred for comparing the average performance of different models [49]. The MAE formula is given in Equation (1).

$$\mathrm{MAE} = \mathrm{n}^{-1} \sum_{\mathrm{i}=1}^{\mathrm{n}} |\mathrm{x_i} - \breve{\mathrm{y}}_\mathrm{i}| \quad (1)$$

n denotes the total number of observations, $\mathrm{x_i}$ is the actual (observed) value for observation i, $\breve{\mathrm{y}}_\mathrm{i}$ is the predicted value for observation i, and $|\mathrm{x_i} - \breve{\mathrm{y}}_\mathrm{i}|$ calculates the absolute difference between these actual and predicted values.

- Mean Square Error (MSE)

The squaring operation used in calculating MSE gives more weight to outliers and large error values. Therefore, MSE can be preferred in determining outliers in the dataset and evaluating the effect of these points on prediction performance. MSE is a measure that

especially emphasises the effect of large errors [50]. The MSE formula is given in Equation (2).

$$\mathrm{MSE} = n^{-1}\sum_{i=1}^{n}(x_i - \breve{y}_i)^2 \quad (2)$$

- Root Mean Square Error (RMSE)

The fundamental assumption when using RMSE is that prediction errors are unbiased and normally distributed. Because of this property, RMSE provides comprehensive information about the overall nature of the error distribution and plays a crucial role in evaluating model performance by assigning greater weight to large errors. Consequently, a low RMSE value indicates higher model reliability and directly reflects prediction quality [51]. The RMSE formula is given in Equation (3).

$$\mathrm{RMSE} = \sqrt{n^{-1}\sum_{i=1}^{n}(x_i - \breve{y}_i)^2} \quad (3)$$

- Coefficient of determination (R^2)

R^2 is a key performance metric that indicates the proportion of total variability in the dependent variable explained by the independent variables. Ranging between 0 and 1, the R^2 value reflects the explanatory power of the model; the closer it is to 1, the greater the model's ability to account for variability in the data. In this context, R^2 plays a critical role in assessing the reliability and predictive accuracy of the model, particularly in regression analyses, by demonstrating how well the model captures the behaviour of the dependent variable [52]. The R^2 formula is given in Equation (4).

$$R^2 = 1 - \frac{\sum_{i=1}^{n}\left(x_i - \breve{y}_i\right)^2}{\sum_{i=1}^{n}\left(\bar{y} - \breve{y}_i\right)^2} \quad (4)$$

x_i represents the actual value of each observation, $\breve{y}_i$ denotes the value predicted by the model, and $\bar{y}$ indicates the mean of all predicted observations.

- Root Mean Square Logarithmic Error (RMSLE)

The RMSLE is a performance metric used to assess a model's sensitivity to large errors and outliers. Specifically designed to emphasize substantial differences between predicted and actual values, RMSLE applies a logarithmic transformation that reduces the impact of small errors while amplifying the effect of larger ones. This characteristic allows for a clearer evaluation of the model's performance in the presence of significant deviations. As a result, RMSLE is particularly useful for assessing model accuracy on datasets with positive and widely varying values [53]. The RMSLE formula is given in Equation (5).

$$\mathrm{RMSLE} = \sqrt{\frac{1}{n}\sum_{i=1}^{n}(\log(1 + \breve{y}_i) - \log(1 + x_i))^2} \quad (5)$$

- Mean Absolute Percentage Error (MAPE)

The MAPE is a key performance metric that expresses prediction error as a percentage of the actual values. Its scale-independent nature enables meaningful comparisons across datasets, making it particularly useful for evaluating and benchmarking model performance. The MAPE formula is given in Equation (6).

$$\text{MAPE} = \frac{100}{n}\sum_{i=1}^{n}\left|\frac{x_i - \breve{y}_i}{x_i}\right| \quad (6)$$

- Task Time (TT (s))

Task Time is a metric that measures how long the model operates, expressed in seconds. This measure is particularly important for evaluating the system's efficiency and speed. A lower Task Time (TT) value indicates faster model execution and improved overall performance.

4. Results and Discussion

All analyses were conducted in Python 3.10.20 using the PyCaret 3.3.2 framework, with standard preprocessing tools (Pandas 3.0.1 [54], NumPy 2.4.0 [55], Seaborn v0.13 [56]). Prior to model training, feature scaling was applied using a standardization procedure (StandardScaler), which transforms each feature independently such that the resulting distribution has a mean (μ) of 0 and a standard deviation (σ) of 1. This process is commonly referred to as Z-score normalization. The models were conducted on a 64-bit Windows operating system running on an Intel® Core™ i7-8565U CPU @ 1.80 GHz with 8.00 GB of RAM, which provided adequate computational resources for the analysis. The dataset was randomly split using an 80/20 hold-out strategy with a fixed random seed of 42, and a 5-fold cross-validation was applied within the training set for model selection and hyperparameter tuning, ensuring an unbiased evaluation on unseen data.

4.1. AutoML Results for Cycle Time Prediction

For cycle time prediction, Table 3 shows that tree-based ensemble models outperformed linear and baseline approaches. In particular, Gradient Boosting and Extra Trees ranked among the best-performing models, indicating their suitability for capturing the non-linear behaviour of the process. Nevertheless, considering the limited dataset size of 81 observations, the results should be interpreted with caution, since high-capacity ensemble models may over-adapt to small datasets if not properly validated [57,58]. Therefore, these findings should be regarded as evidence of modelling potential rather than definitive proof of generalization.

Table 3. Performance metrics for Cycle Time.

Model	MAE	MSE	RMSE	R^2	RMSLE	MAPE	TT (s)
Gradient Boosting Regressor	0.786	2.3626	1.4877	0.9671	0.0081	0.0042	0.028
Extra Trees Regressor	1.0894	5.2288	2.1982	0.9306	0.0119	0.0059	0.044
Bayesian Ridge	1.6972	6.9593	2.5415	0.9238	0.0140	0.0092	0.012
Ridge Regression	1.6500	7.0005	2.5457	0.9226	0.0141	0.0090	0.014
Linear Regression	1.6471	7.0130	2.5480	0.9224	0.0141	0.0090	2.130
Least Angle Regression	1.6471	7.0130	2.5480	0.9224	0.0141	0.0090	0.016
Elastic Net	1.9240	7.5117	2.6541	0.9211	0.0145	0.0104	0.016
Lasso Least Angle Regression	2.0441	8.0248	2.7426	0.9159	0.0149	0.0111	0.012
Lasso Regression	2.0441	8.0248	2.7426	0.9159	0.0149	0.0111	0.810
K Neighbors Regressor	2.2720	8.2455	2.8465	0.9157	0.0153	0.0122	0.014
Huber Regressor	1.2467	7.3735	2.4348	0.9084	0.0139	0.0069	0.018
AdaBoost Regressor	2.1786	9.3231	2.9997	0.9074	0.0160	0.0117	0.032
Random Forest Regressor	1.8681	7.8160	2.7697	0.9056	0.0149	0.0101	0.056
Decision Tree Regressor	1.1411	6.5939	2.3277	0.8973	0.0126	0.0061	0.012
Orthogonal Matching Pursuit	7.0546	67.1484	8.1264	0.3443	0.0429	0.0375	0.014
Passive Aggressive Regressor	7.3506	79.9193	8.6448	0.2168	0.0467	0.0395	0.012

Light Gradient Boosting Machine	9.0982	128.4463	11.0161	−0.103	0.0583	0.0483	0.622
Dummy Regressor	9.3314	136.6438	11.5358	−0.313	0.0612	0.0498	0.014

To assess model reliability and potential overfitting under the limited sample size (N = 81), residual analyses were performed within a 5-fold cross-validation framework (Figure 9). The linear models (Figure 9c,d) exhibit large residual dispersion (up to ±6), whereas the ensemble methods (Figure 9a,b) show tightly centered and pattern-free residuals around zero. In particular, the Extra Trees Regressor (Figure 9b) demonstrates superior stability, with errors confined to approximately ± 0.2. The negligible gap between training and testing performance ($R^2_{train} = 1.00$ and $R^2_{test} = 1.00$) further indicates that overfitting is not evident. Moreover, the similar residual distributions for training and testing sets support that the high accuracy arises from capturing the underlying process behavior rather than memorizing noise, confirming the robustness of the Extra Trees model.

Figure 10 shows the prediction error plots for the regression models. The ensemble methods exhibit the closest agreement with the identity line, with Gradient Boosting (Figure 10a) achieving $R^2 = 0.998$ and Extra Trees (Figure 10b) approaching perfect correspondence ($R^2 = 1.00$). In contrast, the linear models (Figure 10c,d) show noticeably larger scatter and lower determination coefficients ($R^2 = 0.890$ and 0.888, respectively), indicating their limited ability to capture the underlying nonlinear relationships. These trends are consistent with the quantitative metrics and confirm the suitability of ensemble-based models for accurate cycle time prediction under the studied conditions.

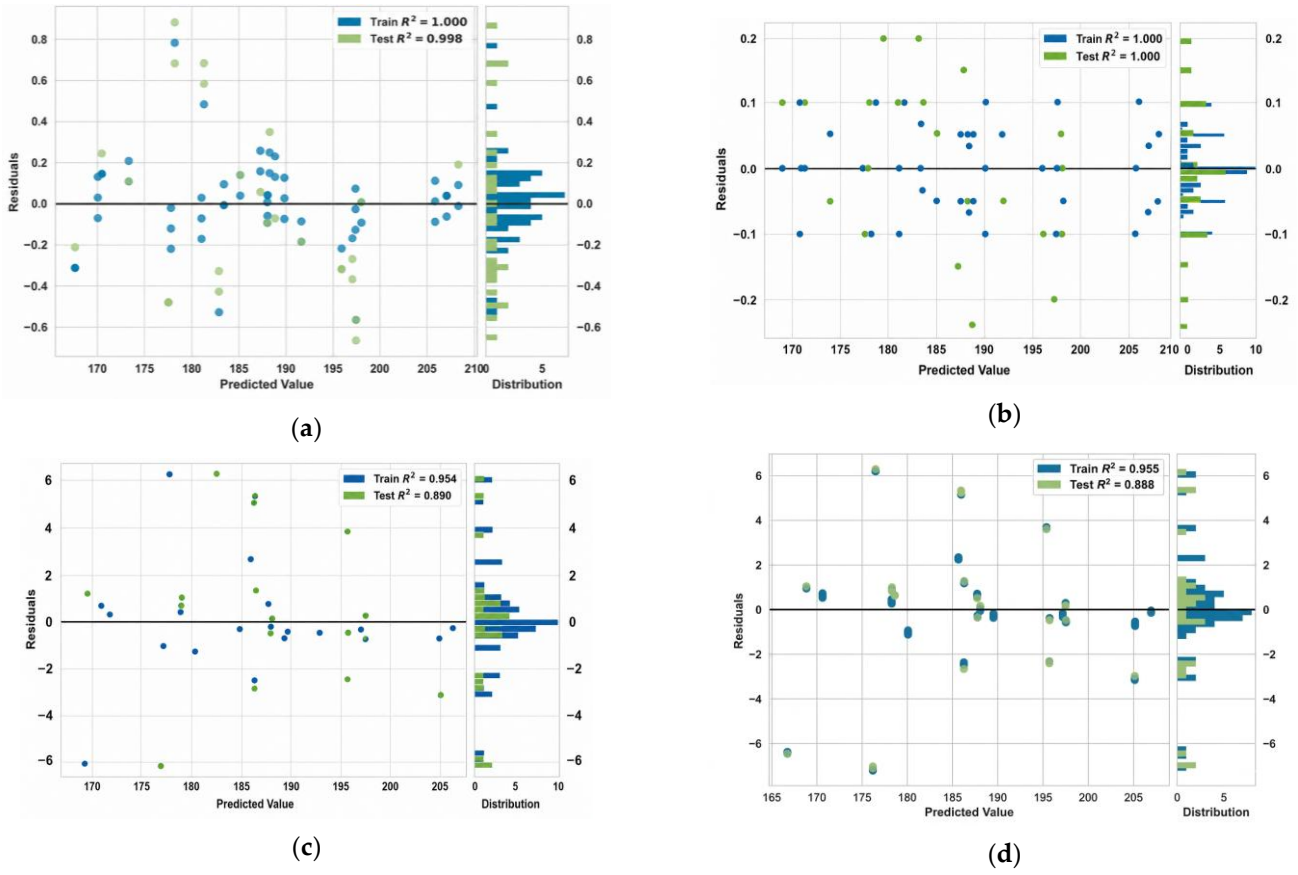

Figure 9. Residual plots of the regression models used for cycle time prediction, including (**a**) Gradient Boosting Regressor; (**b**) Extra Trees Regressor; (**c**) Bayesian Ridge; and (**d**) Ridge Regression.

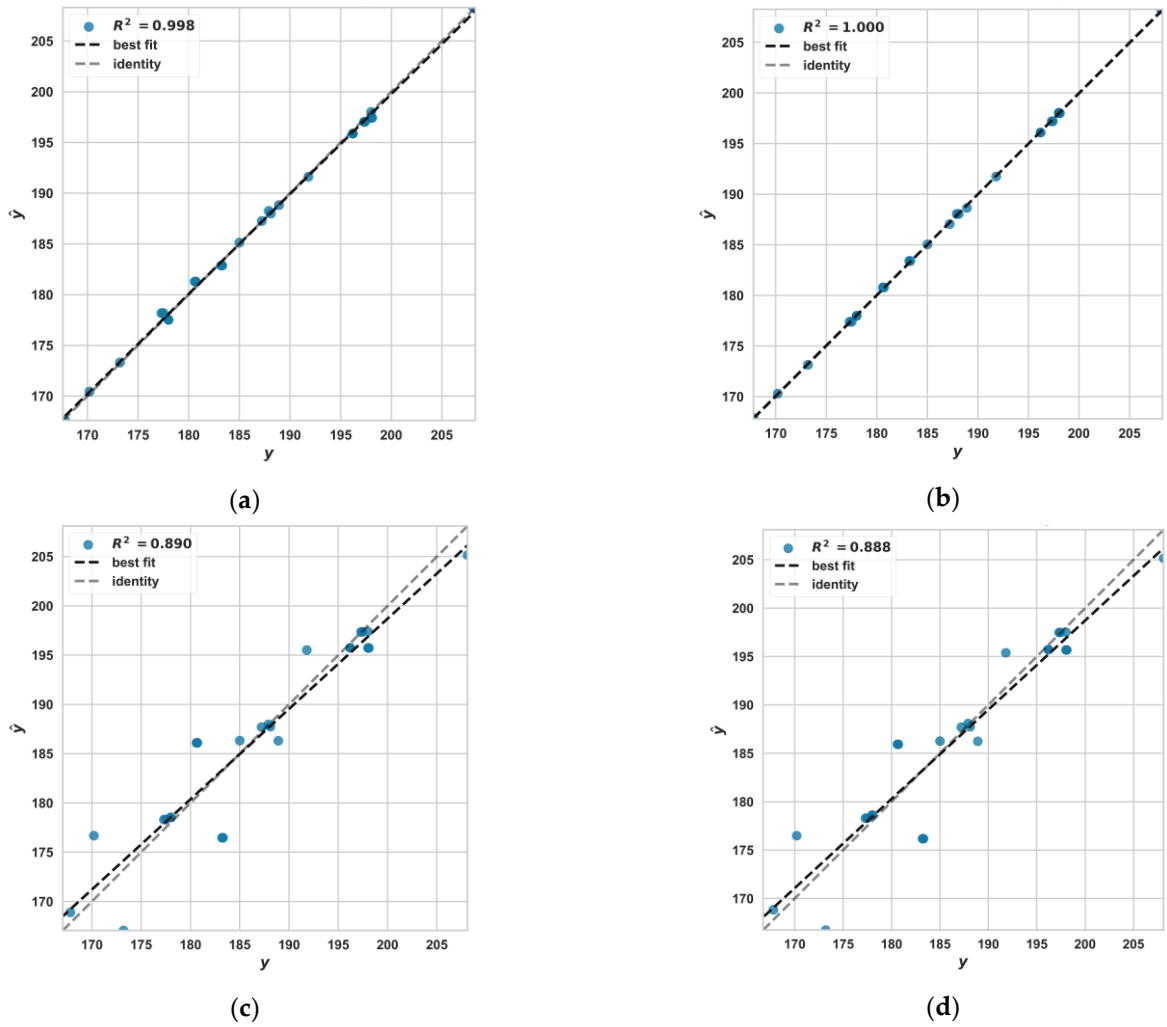

Figure 10. Prediction error plots comparing measured and predicted values for the regression models: (**a**) Gradient Boosting Regressor; (**b**) Extra Trees Regressor; (**c**) Bayesian Ridge; (**d**) Ridge Regression.

Figure 11 summarizes the feature importance results for cycle time prediction. The ensemble models (Gradient Boosting and Extra Trees; Figure 11a,b) concentrate importance on a small subset of variables, with Foam Pressure Cooling Time (P5) and Moving/Fixed Side Cooling Time (P4) emerging as the dominant contributors, indicating that cycle time is primarily governed by a few key parameters. In contrast, the linear models (Bayesian Ridge and Ridge Regression; (Figure 11c,d) distribute importance more evenly across predictors, reflecting their inherent assumptions about correlated features. Despite these differences, all models consistently identify P4 and P5 as the most influential variables, supporting the physical relevance and robustness of these features under the investigated conditions.

To ensure that the feature importance analysis is not distorted by coupling interactions or multicollinearity among the input parameters, a Variance Inflation Factor (VIF) analysis was conducted prior to model training. Because the dataset was generated using an orthogonal Taguchi L27 array, the input parameters are mathematically independent by design. The VIF values for all process parameters (P1–P5) are exactly 1.0. A VIF of 1.0 indicates the complete absence of multicollinearity, ensuring that the tree-based models interpret each parameter's importance objectively, without interference from parameter coupling.

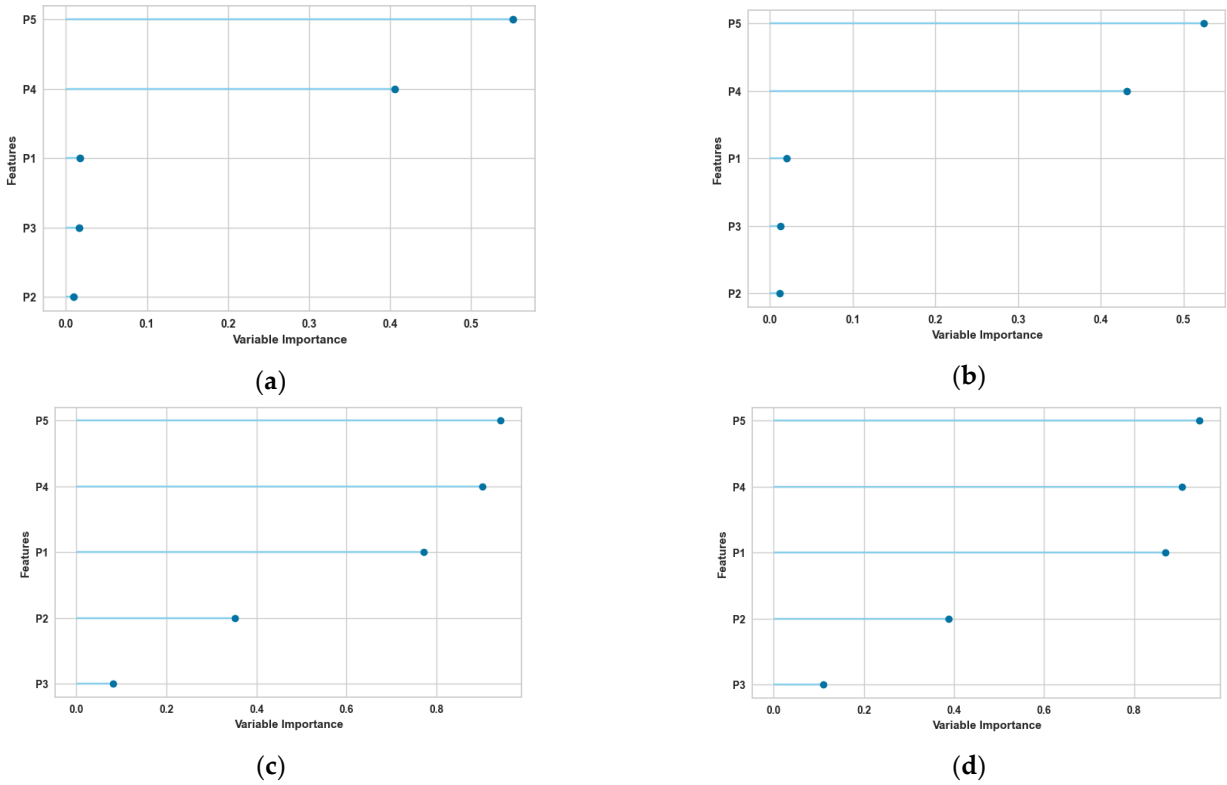

Figure 11. Feature importance analysis for cycle time prediction, including (**a**) Gradient Boosting Regressor; (**b**) Extra Trees Regressor; (**c**) Bayesian Ridge; (**d**) Ridge Regression.

4.2. AutoML Results for Warpage Prediction

Table 4 compares the performance of the AutoML-based regression models for warpage prediction. The Extra Trees Regressor achieves the best overall performance, with the lowest errors (MAE = 0.0995, RMSE = 0.1426) and the highest R^2 (0.9874), indicating a strong ability to capture nonlinear behaviour. The Decision Tree and Gradient Boosting models also perform well ($R^2 > 0.98$), whereas linear methods (e.g., Lasso, Bayesian Ridge, Ridge) show poor accuracy with near-zero or negative R^2 and RMSE values above 1.4. The Passive Aggressive and Light Gradient Boosting models rank among the weakest. Overall, these results confirm the clear advantage of tree-based ensemble methods for warpage prediction. In addition, most high-performing models train in under 0.05 s, demonstrating their practical computational efficiency.

Table 4. Performance metrics for the Warpage.

Model	MAE	MSE	RMSE	R^2	RMSLE	MAPE	TT (s)
Extra Trees Regressor	0.0995	0.0251	0.1426	0.9874	0.0101	0.0074	0.048
Decision Tree Regressor	0.1081	0.0276	0.1551	0.9843	0.0113	0.0082	0.010
Gradient Boosting Regressor	0.1182	0.0294	0.1611	0.9807	0.0113	0.0087	0.026
Random Forest Regressor	0.1439	0.0409	0.1927	0.9796	0.0139	0.0109	0.076
AdaBoost Regressor	0.2112	0.0751	0.2721	0.9593	0.0191	0.0156	0.038
Orthogonal Matching Pursuit	1.2199	2.1284	1.4279	0.0097	0.1009	0.0925	0.012
K Neighbors Regressor	1.0530	2.0106	1.3900	0.0046	0.0992	0.0805	0.012
Lasso Regression	1.2679	2.2931	1.4820	−0.037	0.1045	0.0963	0.010
Lasso Least Angle Regression	1.2679	2.2931	1.4820	−0.037	0.1045	0.0963	0.008
Bayesian Ridge	1.2813	2.3645	1.5009	−0.054	0.1058	0.0974	0.010
Elastic Net	1.2828	2.3358	1.4944	−0.054	0.1054	0.0973	0.008
Ridge Regression	1.2770	2.3188	1.5039	−0.114	0.1051	0.0965	0.008

Linear Regression	1.2760	2.3203	1.5046	−0.115	0.1051	0.0964	0.010
Least Angle Regression	1.2760	2.3203	1.5046	−0.115	0.1051	0.0964	0.008
Dummy Regressor	1.3162	2.5413	1.5571	−0.126	0.1093	0.1002	0.014
Huber Regressor	1.0184	2.7161	1.6151	−0.238	0.1124	0.0828	0.016
Light Gradient Boosting Machine	1.3636	2.6703	1.6117	−0.289	0.1130	0.1034	0.356
Passive Aggressive Regressor	1.9699	5.6667	2.3149	−1.950	0.1606	0.1357	0.010

Figure 12 shows the residual distributions of the four regression models used for warpage prediction. The Extra Trees Regressor Figure 12a exhibits tightly centered, pattern-free residuals around zero (within approximately ±0.1), together with nearly identical training and testing performance ($R^2 \approx 0.999$ and 0.998), indicating excellent generalization. The Decision Tree model (Figure 12b) shows similar but less stable behaviour, with mild clustering at higher predicted values, consistent with localized overfitting in single-tree structures. The Gradient Boosting model (Figure 12c) displays a broader residual spread, suggesting higher sensitivity to sample size and noise accumulation, while the Random Forest model (Figure 12d) yields intermediate performance with larger scatter than Extra Trees. Overall, these results confirm the superior robustness of the Extra Trees approach for reliable warpage estimation under limited data conditions.

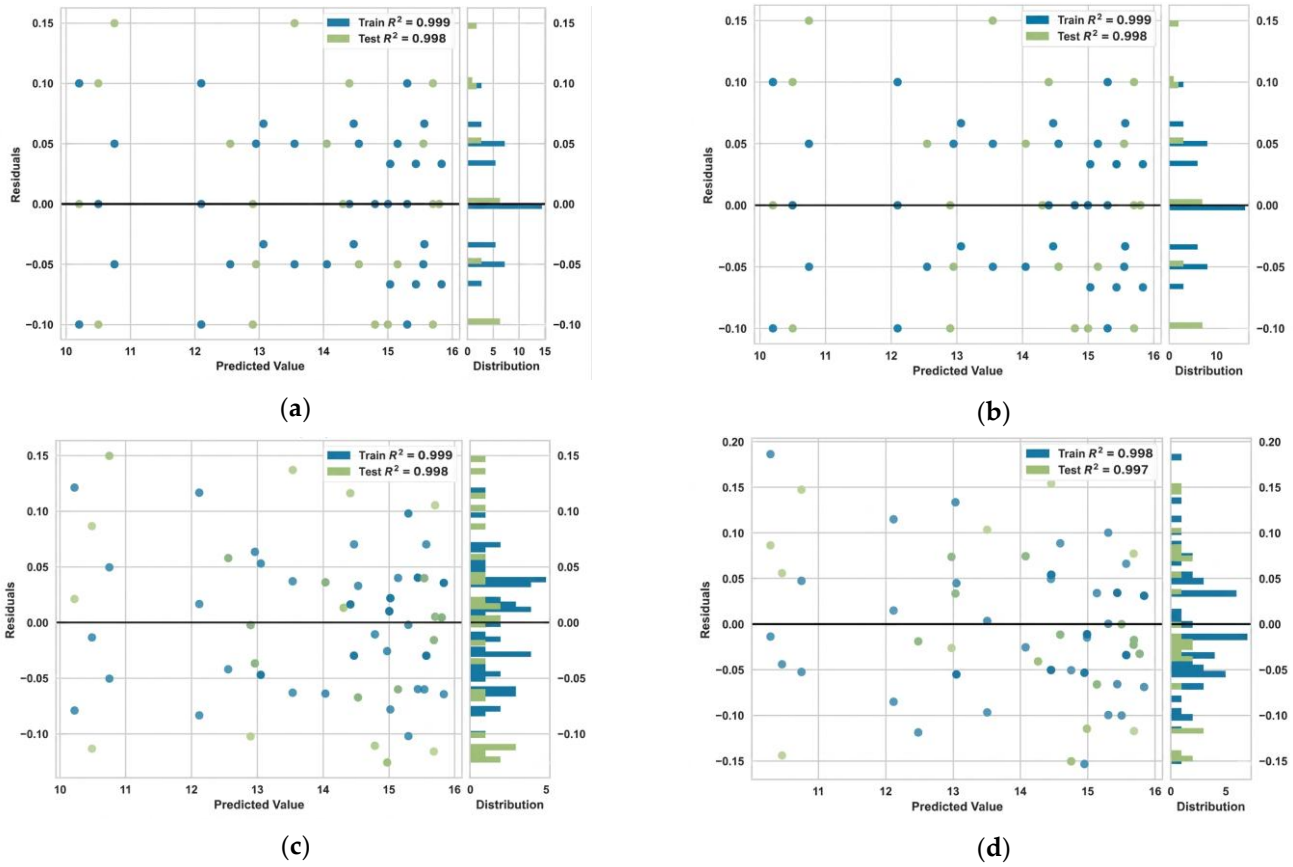

Figure 12. Residual plots of the regression models used for warpage prediction, including (**a**) Extra Trees Regressor; (**b**) Decision Tree Regressor; (**c**) Gradient Boosting Regressor; (**d**) Random Forest Regressor.

As shown in Figure 13, the Extra Trees Regressor (Figure 13a) exhibits the closest agreement between predicted and measured values, with points tightly clustered along the identity line ($R^2 \approx 0.998$) and no evidence of systematic bias. The Decision Tree model (Figure 13b) also shows strong correlation but with slightly increased dispersion, reflecting the sensitivity of single-tree structures to local data partitioning. The Gradient Boost-

ing model (Figure 13c) maintains high accuracy with a modest widening of scatter, suggesting minor cumulative errors due to its sequential learning scheme. The Random Forest model (Figure 13d) achieves comparable performance ($R^2 \approx 0.997$) but with somewhat larger dispersion, indicating reduced precision in capturing fine-scale variations. Overall, these prediction error plots corroborate the residual analysis and confirm that Extra Trees provides the most accurate and robust warpage predictions among the evaluated models.

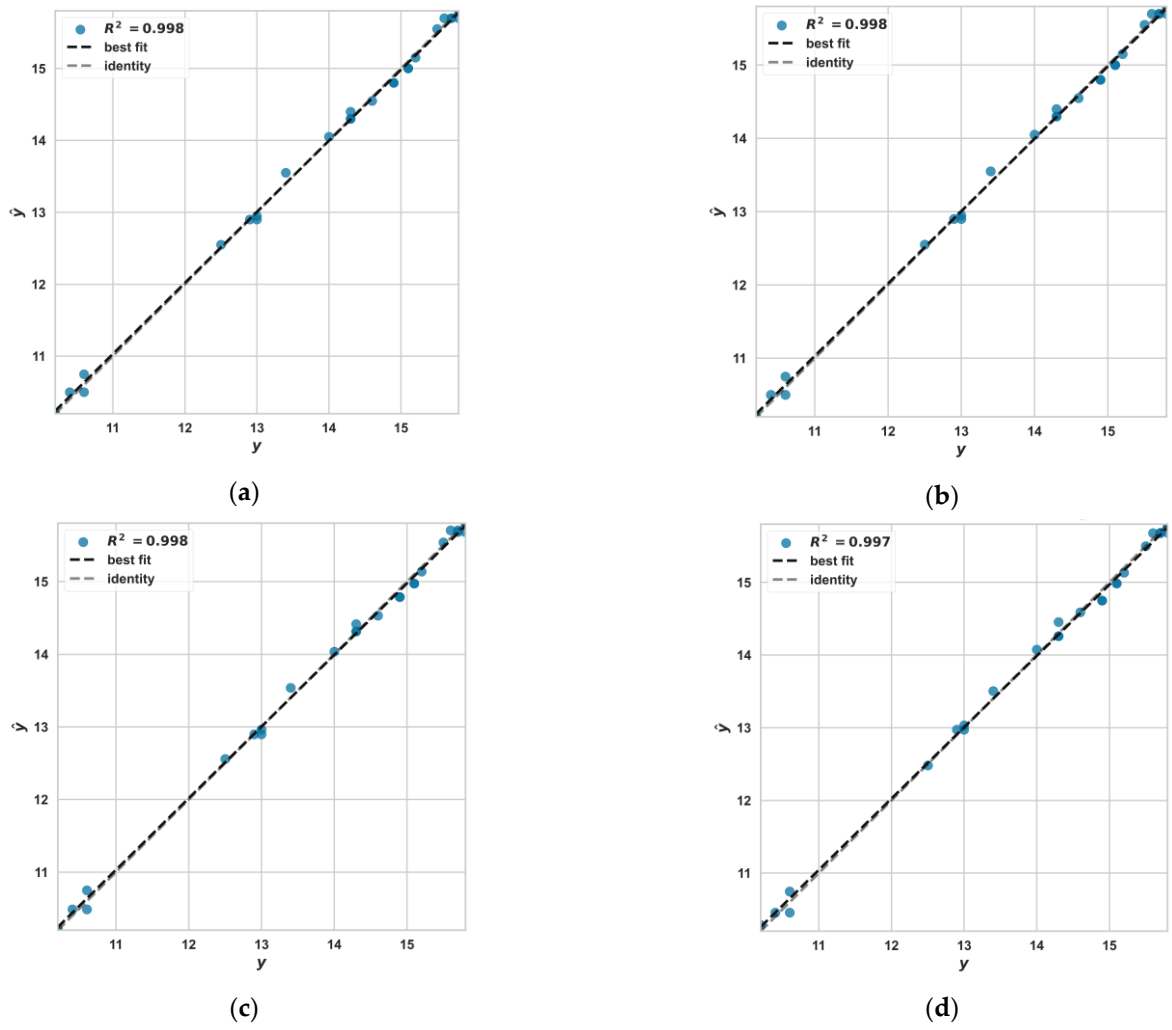

Figure 13. Prediction error plots comparing measured and predicted values for the regression models: (**a**) Extra Trees Regressor; (**b**) Decision Tree Regressor; (**c**) Gradient Boosting Regressor; (**d**) Random Forest Regressor.

Figure 14 illustrates the relative importance of features across the four regression models used for warpage prediction. A clear trend emerges in the Decision Tree, Gradient Boosting, and Random Forest models, where Autoclave Time (P3) and Moving/Fixed Side Cooling Time (P4) are identified as the most significant predictors. In these three cases, Autoclave Time (P3) consistently holds the highest weight, suggesting it is the primary driver of cycle time variability. The high importance assigned to Moving/Fixed Side Cooling Time (P4) across all four algorithms further reinforces its role as a critical parameter. Interestingly, the Extra Trees regressor (Figure 14a) presents a slight deviation from this trend, ranking P1 as the most influential feature, whereas Fixed Side Cross Steam Time (P1) shows significantly less impact in the Decision Tree model. Despite these minor algorithmic variations, there is a consensus regarding the least influential variable: Foam Pressure Cooling Time (P5) consistently ranks at the bottom across all models. This suggests

that Foam Pressure Cooling Time (P5) has a negligible impact on the target output and could potentially be excluded in future model iterations to reduce dimensionality and computational complexity. Overall, the strong agreement between the Gradient Boosting and Random Forest results provides confidence in identifying Autoclave Time (P3) and Moving/Fixed Side Cooling Time (P4) as the core determinants of process warpage.

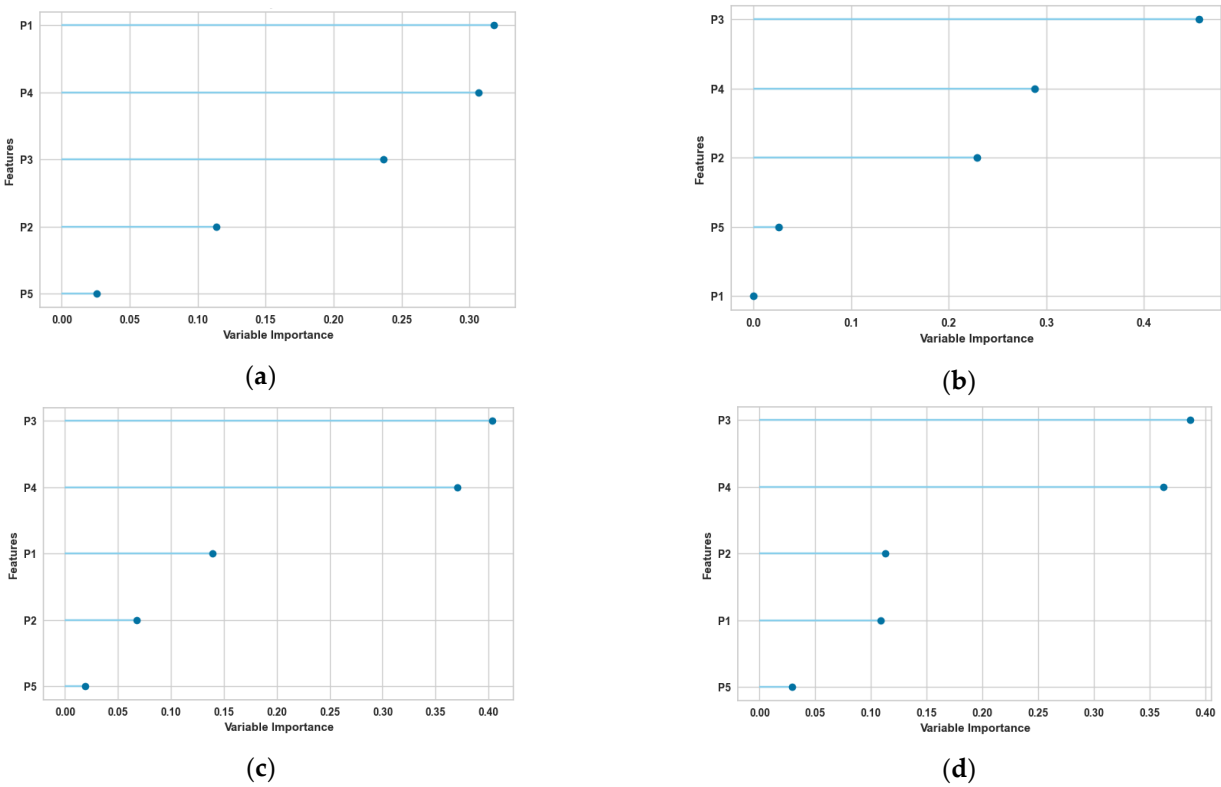

Figure 14. Feature importance analysis for warpage prediction using (**a**) Extra Trees Regressor; (**b**) Decision Tree Regressor; (**c**) Gradient Boosting Regressor; (**d**) Random Forest Regressor.

4.3. Model Robustness Assessment

To evaluate the robustness of the models and address potential concerns regarding model instability due to the relatively small sample size (n = 81), a Repeated 5-Fold Cross-Validation strategy (with 10 repeats) was applied. This approach evaluates each model across 50 distinct training and testing iterations. The performance metrics and their corresponding standard deviations for the top-performing models are presented in Table 5. (for Cycle Time) and Table 6 (for Warpage). The consistently low standard deviations across key metrics confirm that the predictive performance of the selected models is stable and reliable, rather than the result of a specific random data split.

Table 5. RepeatedKFold for cycle time.

Model	MAE	MSE	RMSE	R^2	RMSLE	MAPE
GradientBoosting	0.7860 ± 0.5088	2.3626 ± 3.0922	1.4877 ± 0.9084	0.9671 ± 0.0331	0.0081 ± 0.0050	0.0042 ± 0.0028
ExtraTrees	1.0894 ± 0.5488	5.2288 ± 4.1171	2.1982 ± 1.0540	0.9306 ± 0.0435	0.0119 ± 0.0058	0.0059 ± 0.0030
Bayesian Ridge	1.6972 ± 0.5704	6.9593 ± 4.2899	2.5415 ± 0.8735	0.9238 ± 0.0628	0.0140 ± 0.0048	0.0092 ± 0.0031
Ridge	1.6500 ± 0.7613	7.0005 ± 7.3705	2.5457 ± 1.4042	0.9226 ± 0.1002	0.0141 ± 0.0076	0.0090 ± 0.0042

Table 6. RepeatedKFold for warpage.

Model	MAE	MSE	RMSE	R^2	RMSLE	MAPE
ExtraTrees	0.0995 ± 0.0456	0.0251 ± 0.0291	0.1426 ± 0.0679	0.9874 ± 0.0106	0.0101 ± 0.0051	0.0074 ± 0.0037
DecisionTree	0.1081 ± 0.0452	0.0276 ± 0.0271	0.1551 ± 0.0713	0.9843 ± 0.0121	0.0113 ± 0.0048	0.0082 ± 0.0034
GradientBoosting	0.1182 ± 0.0469	0.0294 ± 0.0303	0.1611 ± 0.0728	0.9807 ± 0.0146	0.0113 ± 0.0052	0.0087 ± 0.0037
Random Forest	0.1439 ± 0.0358	0.0409 ± 0.0218	0.1927 ± 0.0426	0.9796 ± 0.0192	0.0139 ± 0.0031	0.0109 ± 0.0029

In addition to variability arising from data partitioning, the stability of the AutoML-based model selection process itself was further investigated. For this purpose, the entire AutoML pipeline was re-executed using 10 different randomly generated seed values (1091, 688, 1225, 1282, 414, 609, 1038, 905, 994, 744). This procedure introduces controlled stochastic variation in model initialization and data splitting, enabling the assessment of run-to-run consistency. The aggregated performance metrics obtained from these repeated AutoML runs are reported in Table 7 (for cycle time) and Table 8 (for warpage). The relatively low variation observed across these runs indicates that the AutoML framework consistently identifies high-performing models and produces stable predictive outcomes, thereby confirming the robustness of the automated model selection process.

Figure 15 illustrates that the performance advantage of the proposed approach is primarily driven by model class. Linear models (Linear Regression, Ridge, Lasso) consistently underperform relative to tree-based ensembles. For cycle time, Gradient Boosting substantially outperforms Linear Regression, corresponding to an ≈42% reduction in RMSE. This gap is even more pronounced for warpage, where linear models yield negative R^2 values, indicating an inability to capture the underlying process behaviour. Given the inherently nonlinear and interaction-driven nature of the EPP molding process, ensemble methods (Gradient Boosting, Extra Trees) more effectively model these dependencies without explicit feature engineering. Consequently, the advantage of the AutoML framework stems not only from model selection but also from identifying model classes aligned with the process physics.

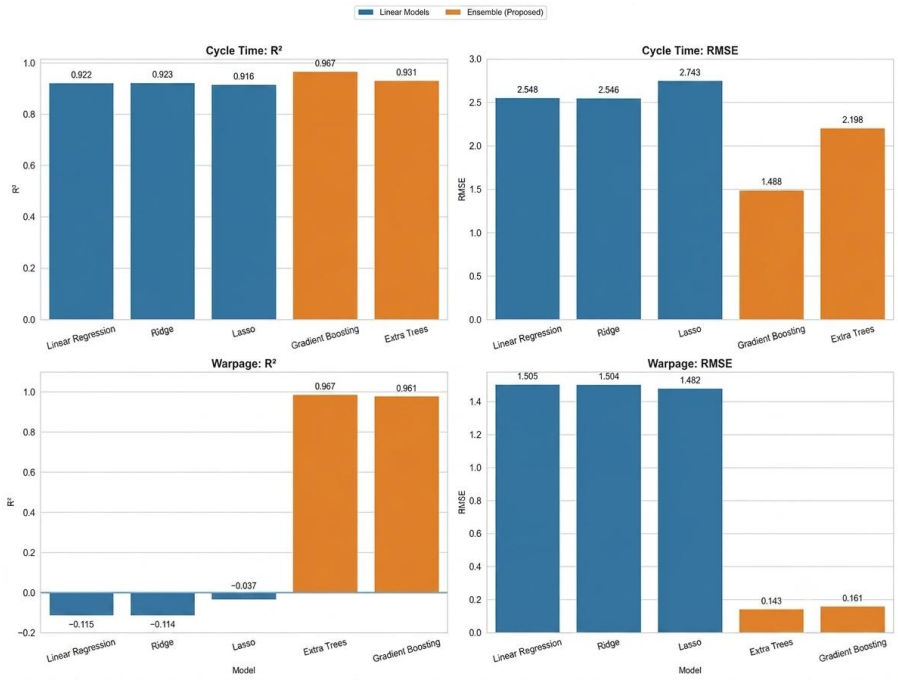

Figure 15. Comparative performance of classical linear models versus proposed ensemble-based models.

Table 7. Performance stability of selected models under repeated AutoML runs (Cycle Time).

Model	MAE	MSE	RMSE	R^2	RMSLE	MAPE
GradientBoosting	0.9396 ± 0.2114	4.0640 ± 1.9455	1.6978 ± 0.3552	0.9590 ± 0.0183	0.0092 ± 0.0018	0.0051 ± 0.0011
ExtraTrees	0.9475 ± 0.2504	4.7249 ± 1.4873	1.8622 ± 0.4405	0.9526 ± 0.0146	0.0102 ± 0.0025	0.0052 ± 0.0014
Bayesian Ridge	2.0698 ± 0.2151	9.1087 ± 1.4862	2.9196 ± 0.2406	0.9111 ± 0.0194	0.0160 ± 0.0013	0.0113 ± 0.0012
Ridge	2.0654 ± 0.2205	9.3143 ± 1.6315	2.9459 ± 0.2585	0.9090 ± 0.0207	0.0162 ± 0.0014	0.0112 ± 0.0012

Table 8. Performance stability of selected models under repeated AutoML runs (Warpage).

Model	MAE	MSE	RMSE	R^2	RMSLE	MAPE
ExtraTrees	0.1116 ± 0.0228	0.0577 ± 0.0805	0.1701 ± 0.0595	0.9743 ± 0.0248	0.0122 ± 0.0044	0.0084 ± 0.0017
DecisionTree	0.1218 ± 0.0157	0.0701 ± 0.1112	0.1881 ± 0.0571	0.9699 ± 0.0287	0.0133 ± 0.0044	0.0090 ± 0.0011
GradientBoosting	0.1230 ± 0.0213	0.0654 ± 0.0985	0.1856 ± 0.0654	0.9735 ± 0.0327	0.0132 ± 0.0048	0.0091 ± 0.0014
Random Forest	0.1651 ± 0.0242	0.0950 ± 0.0925	0.2408 ± 0.0620	0.9571 ± 0.0325	0.0169 ± 0.0048	0.0122 ± 0.0020

4.4. Surrogate Model-Based Process Optimization

To bridge the gap between predictive modelling and industrial process optimization, the finalized surrogate models were employed to explore the global design space of the process. For this purpose, a Monte Carlo-based search was conducted by generating 1000 synthetic experimental trials within the operational boundaries of the five input parameters (P1–P5). Each generated parameter combination was evaluated using the trained surrogate models, and the corresponding cycle time and warpage values were predicted. Since both cycle time and warpage are desired to be minimized, the non-dominated solutions were identified to construct the Pareto front. As shown in Figure 16, the Monte Carlo trials provide a global representation of the feasible prediction space, while the Pareto front indicates the trade-off boundary between productivity and part quality. In the figure, the red star markers represent the selected operating conditions, and the green circles highlight the strictly Pareto-optimal (non-dominated) solutions (settings #1 and #3) that lie directly on the Pareto front. Although setting #2 is among the top three recommended configurations based on the combined normalized objective score, it is technically dominated by setting #1 and therefore does not lie on the Pareto front (hence, it is not enclosed in a green circle). To obtain a practical ranked recommendation for industrial use, the predicted cycle time and warpage values were first normalized using min–max normalization and then combined into a single equal-weight objective score. The objective score was calculated by assigning equal importance to cycle efficiency and dimensional quality. Lower objective scores therefore indicate more favourable operating conditions. Based on this criterion, the top three process parameter combinations were selected from the complete Monte Carlo search space and are presented in Table 9. To further assess the practical validity of the optimization results, the top three recommended parameter configurations were tested on the injection molding machine. The experimentally obtained cycle time and warpage values showed good agreement with the model predictions, supporting the applicability of the proposed surrogate modelling framework under real process conditions. These findings indicate that the AutoML-based surrogate modelling approach can be used not only for predictive purposes, but also for process window identification. By narrowing the feasible design space to a limited number of promising operating conditions, the proposed framework provides actionable process intelligence and helps operators balance cycle time reduction with warpage minimization while reducing the need for extensive additional experimental trials.

Table 9. Top 3 optimal parameter combinations.

Rank	P1	P2	P3	P4	P5	Pred. Cycle Time	Exp. Cycle Time	Pred. Warpage	Exp. Warpage	Obj. Score
1	5.303	5.251	10.939	67.594	33.181	167.671	167.9	10.972	10.81	0.019
2	5.021	6.618	10.852	66.474	31.506	169.441	165.6	11.678	11.05	0.118
3	4.371	5.692	10.859	65.259	31.423	166.051	170.3	12.062	12.08	0.121

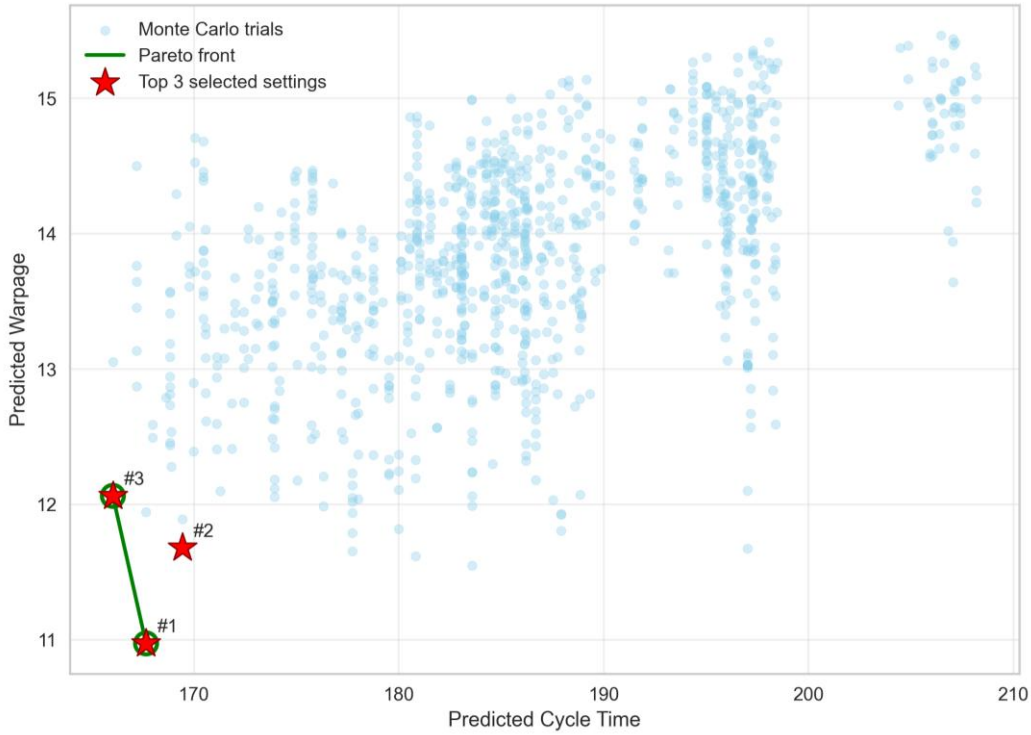

Figure 16. Monte Carlo-Based design space exploration and Pareto Front.

4.5. Extended Benchmarking with Advanced Regression Models

To provide a comprehensive assessment of the predictive framework, the model selection process was extended by incorporating a broader range of regression models. For Cycle Time prediction, the benchmark pool included Gradient Boosting, Extra Trees, Bayesian Ridge, and Ridge Regression, while for Warpage prediction, Extra Trees, Decision Tree, Gradient Boosting, and Random Forest served as the primary candidates. These models were compared against MLP-based neural networks and Gaussian Process Regression (GPR) variants (RBF, Matérn 3/2, Matérn 5/2, Rational Quadratic, and Composite kernels). All models were evaluated using a repeated 5-fold cross-validation strategy with 10 repeats. For Cycle Time prediction, the GPR-Rational Quadratic model achieved an average RMSE of 0.4196 ± 0.6423, MAE of 0.2372 ± 0.3042, and R^2 of 0.9946 ± 0.0182. The Gradient Boosting model, representing the tree-based benchmark, recorded an RMSE of 0.8139. For Warpage prediction, the Extra Trees model recorded an average RMSE of 0.1022 ± 0.0333, MAE of 0.0813 ± 0.0229, and R^2 of 0.9947 ± 0.0044. The most accurate GPR variant, GPR-Matérn 3/2, achieved an RMSE of 0.1058 for the same target variable. These results indicate that GPR variants achieve lower prediction errors for temporal process metrics such as Cycle Time, while tree-based ensemble methods yield higher accuracy for dimensional stability modelling. The inclusion of deep learning architectures and diverse GPR kernels establishes a comprehensive algorithmic benchmark, clarifying the predictive performance of different model families for quality-related outcomes in expanded polypropylene (EPP) injection molding.

4.6. Discussion

The experimental database used in this study was generated using a Taguchi design of experiments, which provides a structured and efficient exploration of the process parameter space. The main motivation for employing AutoML on this dataset is not merely to achieve high predictive accuracy, but also to reduce the need for repeated, time-consuming, and costly physical trials. By enabling reliable surrogate models, the proposed framework supports virtual experimentation, preliminary screening of process conditions, and simulation-based identification of process windows before actual production trials. This approach contributes to shorter development cycles, lower experimental costs, and indirectly to reduced material and energy waste.

In addition to predictive modelling, the finalized surrogate models were further used for multi-objective process optimization through Monte Carlo-based design space exploration. Since both cycle time and warpage are desired to be minimized, non-dominated solutions were identified and represented by the Pareto front. The selected parameter combinations provide practical operating conditions that balance productivity and dimensional quality. Therefore, the proposed framework should not be considered only as a predictive modelling tool, but also as a decision-support approach for process parameter optimization in EPP foam injection molding.

Although the present optimization analysis focuses specifically on cycle time and warpage, broader objectives such as energy consumption, scrap rate, defect rate, and closed-loop process stability were not directly measured in this study. These aspects remain important extensions for future research, particularly through the integration of online sensor data, real-time production monitoring, and adaptive model updating.

Tree-based ensemble methods have demonstrated a statistically significant advantage over classical linear models in predicting complex nonlinear outputs, such as cycle time and warpage, in manufacturing processes. For instance, ensemble models like Random Forest and Gradient Boosting Trees have shown substantial improvements in performance metrics when applied to chemical mechanical polishing using a stacking approach, outperforming single regression models [59]. Likewise, in estimating Overall Equipment Effectiveness (OEE) in an automotive cable production line, Random Forest outperformed both conventional and optimized Support Vector Machine models in terms of accuracy and robustness, contributing to enhanced production efficiency [60]. The effectiveness of these methods stems from their capacity to model multidimensional interactions through flexible tree structures and to reduce prediction variance through ensemble averaging [61,62]. In this regard, tree-based ensemble models offer notable advantages over linear models in terms of generalization performance and estimation stability, particularly under production conditions characterized by multivariate, noisy, and skewed data.

The predictive performance of the proposed AutoML framework (R^2 values of 0.967 and 0.987 for cycle time and warpage, respectively) is highly consistent with the foundational results reported in [17]. In that study, a manually optimized Artificial Neural Network (ANN) achieved peak accuracies of 0.998 and 0.997 on the same dataset. While the specialized ANN in [17] demonstrates the dataset's maximum mathematical precision potential, it inherently functions as a "black box." This study offers critical methodological advancement by shifting from purely predictive deep learning to an automated, interpretable machine learning approach. The AutoML framework ensures near-optimal predictive power while maintaining absolute model transparency through Feature Importance analysis, a crucial requirement for manufacturing engineering. Furthermore, through rigorous overfitting evaluations (i.e., repeated 5-fold cross-validation), we confirmed that the selected models remain structurally robust and capable of true generalization. Consequently, our findings validate that the high accuracy levels established in the literature

can be successfully replicated, objectively verified, and physically explained through automated frameworks, bridging the gap between theoretical mathematical performance and practical, interpretable industrial applications.

5. Conclusions

This study proposes an AutoML-based approach to develop and evaluate data-driven predictive models for the foam injection molding process of EPP, a material widely used in the automotive and packaging industries due to its lightweight structure, impact resistance, and energy absorption capacity. By integrating advanced AutoML techniques with experimental data collected under controlled conditions, this study aimed to overcome the limitations of manual and trial-and-error modelling practices and to support accurate prediction of key quality and performance indicators.

The results indicate that tree-based ensemble models, particularly the Gradient Boosting Regressor, significantly outperform classical regression models in predicting complex output parameters such as cycle time and warpage. These models effectively captured nonlinear relationships within the process, achieving high coefficients of determination ($R^2 \geq 0.96$ for cycle time and $R^2 \geq 0.98$ for warpage) and low error rates. Additionally, their short task times make them suitable for offline or near-real-time decision-support applications, rather than direct closed-loop control.

By automating model selection, hyperparameter tuning, and performance evaluation, the study facilitated a reliable and reproducible comparison of 18 machine learning algorithms. The use of the PyCaret library not only streamlined these processes but also enabled a systematic and objective evaluation of alternative models, allowing users with limited programming experience to implement high-performance predictive models efficiently.

The feature-importance analysis demonstrated that the predictive models captured the underlying physical mechanisms of the EPP molding process, rather than merely identifying statistical correlations. The findings established a clear physical division among the process parameters. Steaming parameters (P1, P2, and P3) govern thermal energy transfer and bead fusion, thereby directly dictating structural consolidation and cycle time. Conversely, cooling and stabilization parameters (P4 and P5) were found to dominate dimensional stability. Because EPP foam has low thermal conductivity, insufficient cooling, and premature demolding trap internal residual stresses. The models correctly identified that these trapped stresses and the resulting differential shrinkage are the primary physical drivers of part warpage.

The computational overhead of the proposed framework is assessed by clearly separating the development and deployment stages. The AutoML search is performed as a one-time, offline procedure to determine the most suitable model architecture, and therefore, it does not introduce any additional burden on the production environment. Once the model is finalized, only the inference phase is executed during operation. In the context of the molding process examined in this study, where the average cycle time is approximately 187.8 s, the inference latency of the selected model, on the order of milliseconds, is effectively negligible. This enables timely parameter adjustments within the practical constraints of the process, without introducing any latency-related limitations. Consequently, the proposed framework is suitable for offline and near-real-time industrial decision-support applications, including potential deployment in edge computing environments.

One limitation of this study is that the industrial mold used for the experiments was not equipped with internal temperature sensors, which prevented the dynamic tracking of mold and coolant temperatures during the process. Therefore, although the proposed models successfully captured the relationships between the selected process parameters

and the output responses, future studies may benefit from integrating additional sensor-based thermal data to improve the physical resolution and adaptability of the modelling framework.

Beyond prediction, this study also demonstrated the practical use of the finalized surrogate models for process window identification through Monte Carlo-based design space exploration and Pareto-front analysis. The selected operating conditions showed that the proposed framework can support industrial decision-making by balancing cycle time reduction and warpage minimization. Future research should therefore focus on extending this framework with online production monitoring, real-time data acquisition, sensor-integrated model updating, and validation across different product geometries, material densities, and mold configurations.

In conclusion, the integration of AutoML frameworks into EPP foam injection molding provides notable advantages in prediction accuracy, model development efficiency, and process decision support. The results indicate that AutoML-based surrogate modelling can serve not only as a predictive tool but also as a practical basis for identifying favorable operating windows in industrial foam molding applications.

Funding: This research received no external funding.

Data Availability Statement: The raw experimental dataset and the scripts developed using Python version 3.10.20 and PyCaret version 3.3.2 are openly available in the following GitHub repository: "https://github.com/enesfurkanerkan/AutoML-Based-Prediction-of-Process-Outcomes-in-Expanded-Polypropylene-Foam-Injection-Molding. (accessed on 2 May 2026).

Conflicts of Interest: There are no conflicts of interest regarding the publication of this paper.

References

1. Pretschuh, C.; Mihalic, M.; Sponner, C.; Lummerstorfer, T.; Steurer, A.; Unterweger, C. Physical Foam Injection Molding of Cellulose Fiber Reinforced Polypropylene by Using CO_2: Parameter Variation and Comparison to Chemical Foam Injection Molding. *J. Compos. Sci.* **2025**, *9*, 50.
2. Jiang, J.; Li, Z.; Yang, H.; Wang, X.; Li, Q.; Turng, L.-S. Microcellular injection molding of polymers: A review of process know-how, emerging technologies, and future directions. *Curr. Opin. Chem. Eng.* **2021**, *33*, 100694.
3. Zhang, A.; Wang, J.; Wang, G.; Jiang, L.; Meng, X.; Zhao, G. Microcellular injection molded lightweight, strong and thermally insulating PP/fibrillated-PTFE composite foams with enhanced surface appearance. *J. Mater. Res. Technol.* **2023**, *22*, 2933–2943.
4. Feng, T.; Guo, W.; Li, W.; Meng, Z.; Zhu, Y.; Zhao, F.; Liang, W. Unveiling Sustainable Potential: A Life Cycle Assessment of Plant–Fiber Composite Microcellular Foam Molded Automotive Components. *Materials* **2023**, *16*, 4952.
5. Saini, R.; Rajak, D.K.; Joshi, T.; Singh, D.K.; Chilla, V.A.N.; Sathaiah, S. Critical review of ultra-lightweight foam materials. *Next Nanotechnol.* **2025**, *7*, 100138.
6. Zhou, Y.; Tian, Y.; Peng, X. Applications and Challenges of Supercritical Foaming Technology. *Polymers* **2023**, *15*, 402.
7. Guo, W.; Mao, H.; Li, B.; Guo, X. Influence of Processing Parameters on Molding Process in Microcellular Injection Molding. *Procedia Eng.* **2014**, *81*, 670–675.
8. Iliadis, D.; Wever, M.; De Baets, B.; Waegeman, W. Hyperparameter optimization of two-branch neural networks in multi-target prediction. *Appl. Soft Comput.* **2024**, *165*, 111957.
9. Thielen, N.; Wagner, M.; Meier, S.; Voigt, C.; Franke, J. Anomaly Detection for Dispensing of Solder Paste on 3D Circuit Carriers Using Machine Learning. In Proceedings of the 2023 IEEE 25th Electronics Packaging Technology Conference (EPTC), Singapore, 5–8 December 2023.
10. Lan, X.; Huang, P.; Chong, Y.; Wu, F.; Su, Y.; Luo, H.; Lee, P.C.; Zheng, W. Autoclave foaming and steam-chest molding of polypropylene/polybutene-1 blend bead foams and their crystallization and mechanical properties. *J. Cell. Plast.* **2023**, *59*, 29–45.
11. Murata, S.; Shioya, S.; Suffis, B. *Expanded Polypropylene (EPP)—A Global Solution for Pedestrian Safety Bumper Systems*; Society of Automotive Engineers: Warrendale, PA, USA, 2004.
12. Xing, Y.; Sun, D.; Zhang, M.; Shu, G. Crushing Responses of Expanded Polypropylene Foam. *Polymers* **2023**, *15*, 2059.

13. Lee, Y.S.; Park, N.H.; Yoon, H.S. Dynamic Mechanical Characteristics of Expanded Polypropylene Foams. *J. Cell. Plast.* **2010**, *46*, 43–55.
14. Bouix, R.; Viot, P.; Lataillade, J.-L. Polypropylene foam behaviour under dynamic loadings: Strain rate, density and microstructure effects. *Int. J. Impact Eng.* **2009**, *36*, 329–342.
15. Shuaeib, F.M.; Hamouda, A.M.S.; Wong, S.V.; Umar, R.S.R.; Ahmed, M.M.H.M. A new motorcycle helmet liner material: The finite element simulation and design of experiment optimization. *Mater. Des.* **2007**, *28*, 182–195.
16. Dixon, D.; Martin, P.J.; Harkin-Jones, E. The Effect of Material Factors on the Density and Cell Morphology of Chemically Foamed Polypropylene. *Cell. Polym.* **2001**, *20*, 403–416.
17. Erkan, N. Parameter Optimization in Foam Injection Process Using Grey Taguchi and Artificial Neural Network Methods. Master's Thesis, Sakarya University, Sakarya, Türkiye, 2024
18. Volpe, V.; Lanzillo, S.; Affinita, G.; Villacci, B.; Macchiarolo, I.; Pantani, R. Lightweight High-Performance Polymer Composite for Automotive Applications. *Polymers* **2019**, *11*, 326.
19. Inayathullah, S.; Buddala, R. Review of machine learning applications in additive manufacturing. *Results Eng.* **2025**, *25*, 103676.
20. Hutter, F.; Kotthoff, L.; Vanschoren, J. (Eds). *Automated Machine Learning: Methods, Systems, Challenges*; Springer: Cham, Switzerland, 2019; p. 219.
21. He, X.; Zhao, K.; Chu, X. AutoML: A survey of the state-of-the-art. *Knowl.-Based Syst.* **2021**, *212*, 106622.
22. Bischl, B.; Binder, M.; Lang, M.; Pielok, T.; Richter, J.; Coors, S.; Thomas, J.; Ullmann, T.; Becker, M.; Boulesteix, A.-L.; et al. Hyperparameter optimization: Foundations, algorithms, best practices, and open challenges. *WIREs Data Min. Knowl. Discov.* **2023**, *13*, e1484.
23. Ashraf, I.; Kehkashan, T.; Zaman, M.; Akhunzada, A.; Talib, H.K.b.; Cao, Y. Enhancing Micro-Expression Recognition with Broadbent Attention Mechanism: A High-Performance Approach for Emotion Detection. In Proceedings of the 2024 IEEE 21st International Conference on Smart Communities: Improving Quality of Life Using AI, Robotics and IoT (HONET), Doha, Qatar, 3–5 December 2024.
24. Khubaib, M.; Kehkashan, T.; Abdelhaq, M.; Khan, M.A.; Zaman, M.; Ashraf, I.; Rehman, A.; Akhunzada, A. Data-Efficient Wheat Disease Detection Using Shifted Window Transformer: Enhancing Accuracy, Sustainability, and Global Food Security. *IEEE Trans. Consum. Electron.* **2025**, *71*, 9006–9020.
25. Kehkashan, T.; Abdelhaq, M.; Al-Shamayleh, A.S.; Huda, N.; Yaseen, I.A.; Ahmed, A.I.A.; Akhunzada, A. Explainable phishing website detection for secure and sustainable cyber infrastructure. *Sci. Rep.* **2025**, *15*, 41751.
26. Azeem, M.; Zaman, M.; Akhunzada, A.; Kehkashan, T.; Ashraf, I.; Rehman, A. Optimizing Diabetic Foot Ulcer Detection: Leveraging SSD and YOLO Architectures. In Proceedings of the 2024 IEEE 21st International Conference on Smart Communities: Improving Quality of Life using AI, Robotics and IoT (HONET), Doha, Qatar, 3–5 December 2024.
27. Párizs, R.D.; Török, D.; Ageyeva, T.; Kovács, J.G. Machine Learning in Injection Molding: An Industry 4.0 Method of Quality Prediction. *Sensors* **2022**, *22*, 2704.
28. Selvaraj, S.K.; Raj, A.; Rishikesh Mahadevan, R.; Chadha, U.; Paramasivam, V. A Review on Machine Learning Models in Injection Molding Machines. *Adv. Mater. Sci. Eng.* **2022**, *2022*, 1949061.
29. Ogorodnyk, O.; Lyngstad, O.V.; Larsen, M.; Wang, K.; Martinsen, K. *Application of Machine Learning Methods for Prediction of Parts Quality in Thermoplastics Injection Molding*; Springer: Singapore, 2019.
30. Ke, K.-C.; Wang, J.-C.; Nian, S.-C. Data-driven quality prediction in injection molding: An autoencoder and machine learning approach. *Polym. Eng. Sci.* **2024**, *64*, 4520–4538.
31. Ke, K.-C.; Wu, P.-W.; Huang, M.-S. Multi-quality prediction of injection molding parts using a hybrid machine learning model. *Int. J. Adv. Manuf. Technol.* **2024**, *131*, 5511–5525.
32. Kuo, C.-C.; Pan, X.-Y. Development of a Rapid Tool for Metal Injection Molding Using Aluminum-Filled Epoxy Resins. *Polymers* **2023**, *15*, 3513.
33. Lee, J.H.; Park, S.; Lim, J.T.; Yoon, H.S.; Choi, J.W.; Ha, C.W.; Park, J. Quick-Delivery Mold Fabricated via Stereolithography to Enhance Manufacturing Efficiency. *Micromachines* **2024**, *15*, 1345.
34. Kuo, C.-C.; Qiu, S.-X.; Yang, X.-Y. A low-cost and highly efficient method of reducing coolant leakage for direct metal printed injection mold with cooling channels using optimum heat treatment process procedures. *Int. J. Adv. Manuf. Technol.* **2021**, *115*, 2553–2570.
35. Kuo, C.-C.; Nguyen, T.-D.; Zhu, Y.-J.; Lin, S.-X. Rapid Development of an Injection Mold with High Cooling Performance Using Molding Simulation and Rapid Tooling Technology. *Micromachines* **2021**, *12*, 311.

36. Hürkamp, A.; Lorenz, R.; Ossowski, T.; Behrens, B.-A.; Dröder, K. Simulation-based digital twin for the manufacturing of thermoplastic composites. *Procedia CIRP* **2021**, *100*, 1–6.
37. Hopmann, C.; Kahve, C.; Schmitz, M. Development of a novel control strategy for a highly segmented injection mold tempering for inline part warpage control. *Polym. Eng. Sci.* **2020**, *60*, 2428–2438.
38. Yin, Y.; Zhai, Z.; Ding, Y. Application of machine learning methods in the analysis of interface bonding strength for overmolded hybrid thermoset-thermoplastic composites. *Polym. Compos.* **2024**, *45*, 8360–8373.
39. Pacella, M.; Mangini, M.; Papadia, G. Utilizing Mixture Regression Models for Clustering Time-Series Energy Consumption of a Plastic Injection Molding Process. *Algorithms* **2023**, *16*, 524.
40. Rohim, M.A.S.; Nazmi, N.; Bahiuddin, I.; Mazlan, S.A.; Norhaniza, R.; Yamamoto, S.-I.; Nordin, N.A.; Abdul Aziz, S.A. Prediction for magnetostriction magnetorheological foam using machine learning method. *J. Appl. Polym. Sci.* **2022**, *139*, e52798.
41. Lacy, F.; Ruiz-Reyes, A.; Brescia, A. Machine learning for low signal-to-noise ratio detection. *Pattern Recognit. Lett.* **2024**, *179*, 115–122.
42. Fushiki, T. Estimation of prediction error by using K-fold cross-validation. *Stat. Comput.* **2011**, *21*, 137–146.
43. Kaczmarczyk, K.; Miałkowska, K. Backtesting comparison of machine learning algorithms with different random seed. *Procedia Comput. Sci.* **2022**, *207*, 1901–1910.
44. Senkaya, M.; Silahtar, A.; Erkan, E.F.; Karaaslan, H. Prediction of local site influence on seismic vulnerability using machine learning: A study of the 6 February 2023 Türkiye earthquakes. *Eng. Geol.* **2024**, *337*, 107605.
45. Zhang, J.M.; Harman, M.; Ma, L.; Liu, Y. Machine Learning Testing: Survey, Landscapes and Horizons. *IEEE Trans. Softw. Eng.* **2022**, *48*, 1–36.
46. Hariri-Ardebili, M.A.; Mahdavi, P.; Pourkamali-Anaraki, F. Benchmarking AutoML solutions for concrete strength prediction: Reliability, uncertainty, and dilemma. *Constr. Build. Mater.* **2024**, *423*, 135782.
47. Salehin, I.; Islam, M.d.S.; Saha, P.; Noman, S.M.; Tuni, A.; Hasan, M.d.M.; Baten, M.d.A. AutoML: A systematic review on automated machine learning with neural architecture search. *J. Inf. Intell.* **2024**, *2*, 52–81.
48. PyCaret. PyCaret Low-Code Machine Learning. Available online: https://pycaret.org/ (accessed on August 2024).
49. Willmott, C.; Matsuura, K. Advantages of the mean absolute error (MAE) over the root mean square error (RMSE) in assessing average model performance. *Clim. Res.* **2005**, *30*, 79–82.
50. Chicco, D.; Warrens, M.J.; Jurman, G. The coefficient of determination R-squared is more informative than SMAPE, MAE, MAPE, MSE and RMSE in regression analysis evaluation. *PeerJ Comput. Sci.* **2021**, *7*, e623.
51. Chai, T.; Draxler, R.R. Root mean square error (RMSE) or mean absolute error (MAE)? *Geosci. Model Dev.* **2014**, *7*, 1247–1250.
52. Mustain, B.C. Correlation and Causation. *Sci. News* **1982**, *121*, 387.
53. Ahmadi, B.; Gholamalifard, M.; Ghasempouri, S.M.; Kutser, T. Comparative assessment of machine learning algorithms for retrieving colored dissolved organic matter (CDOM) from Sentinel-2/MSI images in the coastal waters of the Persian Gulf. *Ecol. Inform.* **2025**, *89*, 103171.
54. Christ, M.; Braun, N.; Neuffer, J.; Kempa-Liehr, A.W. Time Series FeatuRe Extraction on basis of Scalable Hypothesis tests (tsfresh—A Python package). *Neurocomputing* **2018**, *307*, 72–77.
55. Harris, C.R.; Millman, K.J.; van der Walt, S.J.; Gommers, R.; Virtanen, P.; Cournapeau, D.; Wieser, E.; Taylor, J.; Berg, S.; Smith, N.J.; et al. Array programming with NumPy. *Nature* **2020**, *585*, 357–362.
56. Stančin, I.; Jović, A. An overview and comparison of free Python libraries for data mining and big data analysis. In Proceedings of the 2019 42nd International Convention on Information and Communication Technology, Electronics and Microelectronics (MIPRO), Opatija, Croatia, 20–24 May 2019.
57. Hastie, T.; Tibshirani, R.; Friedman, J. *The Elements of Statistical Learning*; Springer: New York, NY, USA, 2009.
58. Hawkins, D.M. The Problem of Overfitting. *J. Chem. Inf. Comput. Sci.* **2004**, *44*, 1–12.
59. Li, Z.; Wu, D.; Yu, T. Prediction of Material Removal Rate for Chemical Mechanical Planarization Using Decision Tree-Based Ensemble Learning. *J. Manuf. Sci. Eng.* **2019**, *141*, 031003.
60. Hassani, I.E.; Mazgualdi, C.E.; Masrour, T. Artificial Intelligence and Machine Learning to Predict and Improve Efficiency in Manufacturing Industry. *arXiv* **2019**, arXiv:1901.02256.
61. Merghadi, A.; Yunus, A.P.; Dou, J.; Whiteley, J.; ThaiPham, B.; Bui, D.T.; Avtar, R.; Abderrahmane, B. Machine learning methods for landslide susceptibility studies: A comparative overview of algorithm performance. *Earth-Sci. Rev.* **2020**, *207*, 103225.
62. Fan, J.; Yue, W.; Wu, L.; Zhang, F.; Cai, H.; Wang, X.; Lu, X.; Xiang, Y. Evaluation of SVM, ELM and four tree-based ensemble models for predicting daily reference evapotranspiration using limited meteorological data in different climates of China. *Agric. For. Meteorol.* **2018**, *263*, 225–241.

https://doi.org/10.3390/machines14070797